國立交通大學

機械工程學系

博士論文

光學玻璃模造成形之有限元素分析

Finite Element Analysis on the Optical Glass Molding Process

研究生：蔡宇中

指導教授：洪景華　教授

中華民國　九十九年六月

光學玻璃模造成形之有限元素分析

Finite Element Analysis on the Optical Glass Molding Process

研 究 生：蔡宇中　　Student：Yu-Chung Tsai

指導教授：洪景華　　Advisor：Chinghua Hung

國 立 交 通 大 學

機 械 工 程 學 系

博 士 論 文

A Dissertation

Submitted to Department of Mechanical Engineering

College of Engineering

National Chiao Tung University

in partial Fulfillment of the Requirements

for the Degree of

Doctor of Philosophy

in

Mechanical Engineering

June 2010

Hsinchu, Taiwan

中華民國九十九年六月

光學玻璃模造成形之有限元素分析

研究生: 蔡宇中　　指導教授: 洪景華 教授

國立交通大學機械工程學系

摘要

玻璃模造技術為一適合用於大量製造內嵌在 3C 產品中的光學元件(如手機相機模組中的光學玻璃透鏡)之量產方式。儘管此技術具備許多優勢，在實際製造上仍有許多困難需克服。其中最關鍵的問題為歷經製程後的透鏡成品與原始設計值之間存在誤差。為解決此問題，本研究以詳盡的材料模型建立有限元素分析模型，並以此模型預測光學玻璃模造後之透鏡成品外型，期能藉此分析指出此問題關鍵處並加以改善。

為建構一完整的光學玻璃模造成形之有限元素分析模型，本研究一開始即針對玻璃進行材料實驗以取得詳盡的材料性質。研究裡採用的是低玻璃轉移溫度之玻璃 L-BAL42 (Low T_g glass, T_g=506°C, Ohara Co.)。藉由熱膨脹實驗，得到玻璃在液體和玻璃態下的熱膨脹係數。接著利用掃描式熱差分儀（DSC）和單軸壓縮應力鬆弛實驗，分別取得玻璃之結構鬆弛性質以及應力鬆弛性質。另在成形溫度（568℃，At + 30℃）下進行單軸壓縮試驗，驗證牛頓流體確實能夠準確地代表玻璃在成形階段的流動行為。最後進行一非球面光學玻璃透鏡成形實驗，並以此實驗之成形參數代入分析中。分析模型以商用有限元素軟體 MARC 建立，並代入玻璃材料實驗所得之材料性質。藉由模擬和實驗結果比對一致性與準確性，確認了本研究提出之光學玻璃模造成形有限元素分析模型。

關鍵字: 光學玻璃透鏡，玻璃模造成形，有限元素分析，熱膨脹，單軸壓縮，牛頓流體，結構鬆弛，應力鬆弛。

FINITE ELEMENT ANALYSIS ON THE OPTICAL GLASS MOLDING PROCESS

Student: Yu-Chung Tsai Advisor: Prof. Chinghua Hung

Department of Mechanical Engineering

National Chiao Tung University

ABSTRACT

Glass molding is a high-volume fabrication method suitable for producing optical components embedded in 3C products, such as optical glass lenses in the camera modules of mobile phones, digital cameras and projectors, etc. Despite the advantages of glass molding, several difficulties encountered in the manufacturing process have yet to be overcome. The most critical issue is the deviation between the formed lens and the original lens shape design. Thus, to overcome this obstacle, the focus of this dissertation is to introduce finite element analysis (FEA) into the prediction of the molded lens shape with detailed material models of the optical glass.

To construct a comprehensive finite element (FE) model for the optical glass molding process, this study firstly performed experiments on the optical glass to obtain detailed material properties. Low T_g optical glass, L-BAL42 (T_g=506°C, Ohara Co.), was used in this research. Detailed thermal expansion coefficients including liquid and glassy states are obtained by thermal expansion experiment. Followed by using differential scanning calorimetry (DSC) and uniaxial compressive stress relaxation experiments, the structural relaxation property and the stress relaxation property were obtained respectively. Uniaxial compression test was also performed at

the molding temperature (568°C, 30°C above At) to verify that the Newtonian fluid could accurately represent the glass flow behavior at molding stage. An aspherical optical glass lens molding experiment was then performed and the FEA with the same forming parameters was also conducted by using the commercial finite element program, MARC, incorporating these obtained material properties and the proposed material model. After verifying the consistency of simulation and experimental results, a comprehensive FE model for optical glass lens molding process was assured.

Keywords: *Optical glass lens, glass molding, finite element, thermal expansion, uniaxial compression, Newtonian fluid, structural relaxation, stress relaxation.*

誌謝

首先要感謝指導教授，洪景華老師，從我碩士班一路到博士班，一共九年的時光，不厭其煩、不辭辛勞的在研究的路途上引導我，在研究過程中各個關鍵時刻拉拔我，讓我順利完成學業，邁入人生下一個階段。遇到一個這麼好的師父，是我這一生中最幸運的一件事。

非常感謝口試委員黃佑民教授、徐瑞坤教授、宋震國教授、賀陳弘教授和黃國政博士。感謝你們提出的諸多建議，讓我的論文更臻完整。

儀科中心曾釋鋒先生、黃建堯先生、郭朝輝先生，非常感謝三位在百忙中仍抽空協助我進行實驗，讓我能順利完成研究。

感謝洪榮崇學長，不但在研究上提供實驗機台和許多寶貴的建議，在研究之外也不忘照顧我、提點我，讓我這九年的求學之路走得更為順遂。除了父母之外，最照顧我的，當屬待我如親兄弟的洪榮崇學長了。

實驗室的學弟妹們:雅雯、建溢、奇忠、政成、琇晶、維德、智偉、煌棊、正展、銘傑、麒禎、嘉偉、理強、宗駿、彥彬、黃詠、世璿、運賢、志嘉、俊羿、志傑、聖平、時恆、建榮、麒翔、忠諭、宗錞、筱瑋、立釗、正一、振傑、雅喬、中南、書麟、馨云。感謝你們多年來一直容忍我作威作福，對你們做出各式威脅逼迫的動作。恭喜你們，終於脫離威權，迎向民權了!

交大十三年，研究所九年，一路走來雖有些許顛簸，但仍算極為順遂。特別是路途中遇到的諸多貴人，讓我無論在研究上或生活上都能順利過關。對於諸位，在此僅以感恩二字表達最衷心的感激之意。

最後，非常感激我的家人，特別是我的父母，在我的求學過程中無怨無悔的支持我，給我最大的自由度去探索這個世界。非常榮幸能作你們的兒子，感謝你們!

TABLE OF CONTENTS

LIST OF TABLES

LIST OF FIGURES

NOMENCLATURE

A	Two planes of area
A_4	Fourth order coefficient of aspherical equation
A_6	Sixth order coefficient of aspherical equation
A_8	Eighth order coefficient of aspherical equation
A_{10}	Tenth order coefficient of aspherical equation
a	Optical glass sample thickness
c	Difference in the photoelastic constants
C_p	Heat capacity
C_{pg}	Heat capacity of the glassy state
C_{pl}	Heat capacity of the liquid state
d	Distance between two planes
E	Elastic modulus
E	Calibration constant
F	Force
G	Shear modulus
H	Heat flow
H_e	Equilibrium enthaply
Hr	Heating rate
ΔH	Activation energy
K	Conic constant
k_m	Shear strength
M	Sample mass
M_p	Response function

m	Shear friction factor
q	Cooling rate
R	Radius of curvature
R	Gas constant
r	Distance from the lens axis in the radial direction
s	Residual stress
T	Temperature
T_0	Initial temperature
T_f	Fictive temperature
T_g	Transition temperature
T_L	Lower temperature limit
T_{ref}	Reference temperature
T_U	Upper temperature limit
t	Time
V	Volume
v	Velocity
w_g	Weighing factor of structural relaxation
w_i	Weighing factor of stress relaxation
x	Fraction parameter
z	Aspherical surface profile
α_l	Linear liquid coefficient of thermal expansion
α_g	Linear solid coefficient of thermal expansion
α_{vl}	Volumetric liquid coefficient of thermal expansion
α_{vg}	Volumetric solid coefficient of thermal expansion
β	Phenomenological parameter

ε	Strain
ε_{12}	Shear strain
ε_{12}^{E}	Shear strain (elastic behavior)
$\dot{\varepsilon}_{12}^{E}$	Shear strain rate (elastic behavior)
$\dot{\varepsilon}_{12}^{V}$	Shear strain rate (viscous behavior)
ε^{th}	Thermal strain
η	Viscosity
η_0	Pre-exponential factor
λ	Wavelength of light
λ_s	Retardation time
ν	Poisson's ratio
σ	Stress
σ_{11}	Normal stress
σ_{12}	Shear stress
σ_{12}^{E}	Shear stress (elastic behavior)
σ_{12}^{V}	Shear stress (viscous behavior)
τ_p	Property relaxation time
$\tau_{p.ref}$	Reference property relaxation time
τ_s	Stress relaxation time
τ_v	Structural relaxation time
ξ	Reduced time
Ψ	Stress relaxation function

CHAPTER 1 INTRODUCTION

1.1 Introduction

With the improvement of technology, more and more optical lenses are widely used in various optical or optoelectronic systems. Application fields of these optical lenses range from military equipments (laser rangefinder, periscope etc.), to medical equipments (endoscope, eye magnifier etc.), to industrial usage (optical fiber communication), and to 3C products (mobile phones, digital cameras and projectors etc.). The requirement on optical lenses is increasing rapidly. Moreover, with the growth of the consumer electronics market, demands on light weight, compact, portable and high performance products are increased. These all lead into an issue: to produce optical lenses in high quantities and retain their high optical performances in the meantime.

Two kinds of materials, optical polymer and optical glass, are widely used to fabricate most optical lenses. Optical polymers have been used for years to produce optical lenses, prisms, gratings and light guides etc. The main advantages of polymers are their light weight and ease of mass production by injection molding or hot embossing. Optical glass on the other hand has higher transparency, higher scratch and humid resistance. Another advantage of the optical glass is that its thermal expansion coefficient (α) is approximately one order of magnitude smaller than the thermal expansion coefficient of the optical polymers (10^{-6}/°C vs. 10^{-5}/°C). This reduces difficulties in designing high precision optical systems. Moreover, one of the major optical properties, the refractive index of the optical glasses ranges from 1.5 to over 2.0 while the refractive index of the polymers ranges from 1.3 to 1.7. Higher refractive index exhibits greater capability to bend the light rays to focus in a narrow

range thus provides larger applications of the optical lenses. The above mentioned advantages make optical glass suitable for high precision applications.

1.2 Optical Glass Lenses and Traditional Fabrication Methods

Traditional grinding-and-polishing method, comprising several steps: pre-forming, lapping, polishing and centering, is widely used to fabricate the optical glass lenses. Because the movements of the pre-forming tool (as shown in Figure 1.1) and the polishing tool (as shown in Figure 1.2) are fixed to swing spherically, the traditional fabrication method was limited to form the spherical lenses. Besides, the usage of the spherical lens is also limited owing to one of its drawbacks, the spherical aberration. Because of the spherical shape of the lens, the focal point of the light rays away from the lens axis is near than that of the rays closer to the lens axis, thus results in blur of the image. Figure 1.3a shows the schema of the phenomenon of the spherical aberration. In most applications, spherical aberration is eliminated by arranging multiple spherical lenses in a row to compensate the errors introduced by each other, as shown in Figure 1.3b. However, adding lens elements results in mounting and alignment complexities, heavier weight and higher costs. To make the product lighter, smaller and cheaper, aspherical lenses are the ideal choices since they are able to focus all the incident lights on a single point of the lens axis without additional error-correcting lenses for optical assemblies, as Figure 1.4 shows.

The production of aspherical glass lenses using traditional grinding-and-polishing method is much difficult than for spherical lenses. Computer numerically controlled (CNC) generator is used recently to fabricate the aspherical lens. Also, ultra-precision grinding is implemented to generate the desired shape on the glass lenses. However, both CNC generating and ultra-precision grinding are time-consuming and expensive which cannot meet the requirement of mass production. New approach must be

proposed to deal with this obstacle.

1.3 Glass Molding Technology

Glass molding technology was first proposed in the US patent 3833347 [5] in 1974 by Eastman Kodak. The feature of the technology is to form the optical glass lenses into a desired shape with an open or closed mold by reheating their preform to a specified temperature, which is lower than the glass fused temperature but higher than the glass transition temperature. Due to large developing expenses and low fabricating accuracies at that time, this technology is not introduced into manufacturing process until the last few years.

Unlike traditional grinding-and-polishing method, glass molding simplified the forming procedures into a three-stage sequential process including, heating, molding, and annealing, as shown in Figure 1.5. In the heating stage, both the molds and glass preform are heated to a specified temperature, defined as the molding temperature, which is usually above the glass transition temperature (T_g) or the yield point (At). In the molding stage, a preset force (or displacement) is applied to the glass preform with an open or closed die setting. In the final annealing stage, the molds are held at the end position of the forming stage until they reach the mold-releasing temperature. The formed lens separates from the molds upon reaching the releasing temperature. Figure 1.6 shows the schema of the processing history. Via glass molding, various optical lenses such as bi-convex lens, bi-concave lens, meniscus lens, insertion lens, f-θ lens, micro lens array and fiber array etc., as shown in Figure 1.7, can be mass-produced.

1.4 Finite Element Analysis on the Glass Molding Process

Despite the advantages of the glass molding process, several difficulties have yet to be overcome. The most critical obstacle is that the formed lens shape often deviates

from the original design, leading to poor optical quality. In current industrial practice, engineers must modify molds several times through trial and error to achieve the desired lens shape. This procedure must be repeated for each type of glass material, causing unwanted time costs. This is especially troublesome for the short life cycles typical of 3C products.

Finite element analysis (FEA) has been widely used to analyze the manufacturing process or the product performance. With the aid of FEA, it is easier to observe the problems and to make strategies on the resolution without time-consuming trial-and-error method. Optical glass lens molding process can also utilize FEA to overcome encountered obstacles. To realize this idea, a comprehensive FEA model of the optical glass lens molding process must be established and be confirmed.

1.5 Literature Reviews

Material models are the key factors that decisively affect the accuracy of the FEA result. Gy [7] and Duffrène et al. [8],[9] regarded glass as a viscoelastic material and have focused on its stress relaxation behavior with several mathematical and experimental works. Hyre [10] discussed the bottle formation of glass at a high temperature and regarded the glass as a Newtonian fluid. The rigid-viscoplastic material model was usually introduced into FEA to describe the flow behavior of the glass. Zhou et al. [11] discussed the viscoelastic behaviors, especially the stress relaxation behavior, of a low T_g glass at several temperatures close to the molding temperature.

Using FEA, a group in the Ohio State University addressed on several issues [12]-[17] in the glass molding process at temperatures approximately 100°C above T_g. However, some low T_g optical glasses widely used by the industry, heated to 100°C above T_g are very close to their softening point (SP) which might cause the glasses to

deform under their own weight. This phenomenon makes the molding process more difficult to control. Therefore, the molding temperature adopted by the industry is usually 30°C above At (or 50~60°C above T_g). Another benefit is that lower temperature processes lengthen the operating lifetime of the molds [18].

Jain [2] first introduced complete glass material properties, i.e. linear coefficient of thermal expansion, Newtonian fluid behavior, structural relaxation, and stress relaxation into FEA on the glass molding process to predict the molded lens surface curve. But these properties were obtained from empirical assumptions by referring to references rather than experimental works. These may not suitable for other types of glass materials. To construct a comprehensive FE model for the glass molding process with specified optical glass, detailed material properties should be obtained from material experiments.

1.6 Scope of the Present Study

Despite the above mentioned efforts on introducing FEA into glass molding process, a complete and accurate FE model based on the industrial forming conditions has not yet been proposed. Therefore, the objective of this study is to construct a comprehensive FE model with detailed material properties of the optical glass obtained from material experiments. Because the most critical issue of the obstacles in the molding process is the deviation between the formed lens and the original lens shape design, this study also uses the constructed FE model to predict the molded optical glass lens shape and attempts to indicate the key factors to resolve this difficulty.

In order to construct a comprehensive FE model for the optical glass molding process, this study firstly performed material experiments to obtain detailed properties of the optical glass. Low T_g optical glass L-BAL42 (T_g=506°C, Ohara Co.) was used in this research. Detailed thermal expansion coefficients including liquid and glassy

states are obtained by thermal expansion experiment. Followed by differential scanning calorimetry (DSC) and uniaxial compressive stress relaxation experiment, the structural relaxation property and the stress relaxation property were obtained respectively. Uniaxial compression experiment was also performed at the molding temperature (568°C, 30°C above At) to verify that the Newtonian fluid could accurately represent the glass flow behavior at molding stage. An aspherical optical glass lens molding experiment was then performed and the FEA with the same forming parameters was also conducted by using the commercial finite element program, MARC, incorporating these obtained material properties and the verified material model. After verifying the consistency of simulated and experimental results, a comprehensive FE model for optical glass lens molding process was assured.

1.7 Structure of Dissertation

This chapter introduces the background of glass molding technology and the efforts on how to apply FEA on the glass molding process. Chapter 2 describes the glass behaviors in the glass transition region, where the molding process is preformed. Detailed optical glass material models for the FEA in each forming stages of the molding process are also discussed. Chapter 3 describes the material property experiments for constructing these material models. Verification on the usage of Newtonian fluid as the glass behavior in the molding stage and the comparison and discussion between the formed lens shape of the molding experiment and the FEA results are included in chapter 4. Finally, chapter 5 concludes and summaries this study.

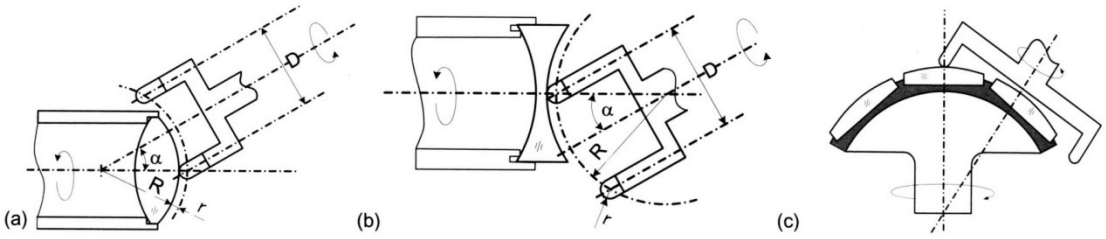

Figure 1.1 Cup shape diamond grinding tool conducting (a) concave (b) convex (c) multi-lens pre-forming process [1].

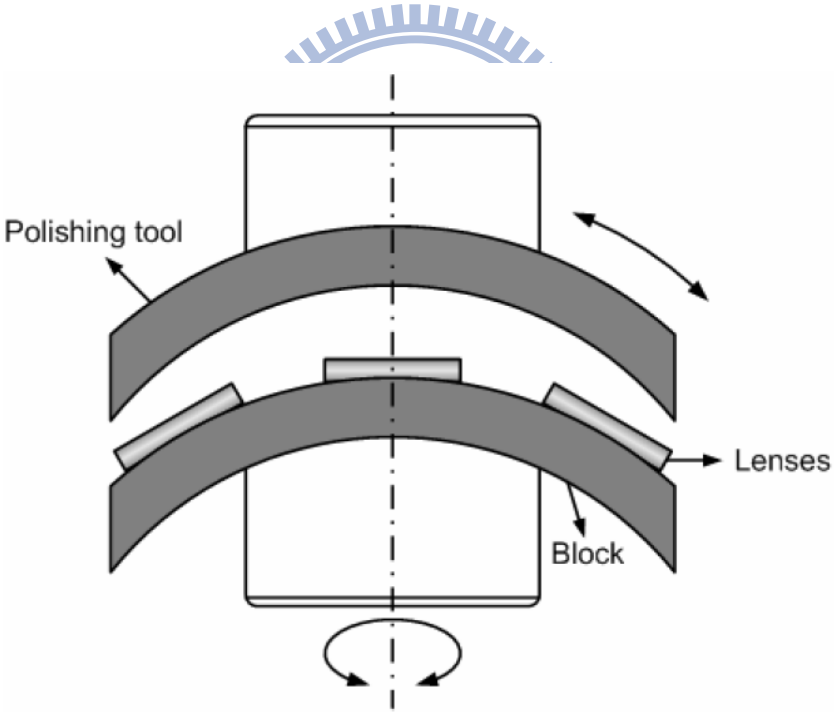

Figure 1.2 Schema of the traditional polishing process [2]

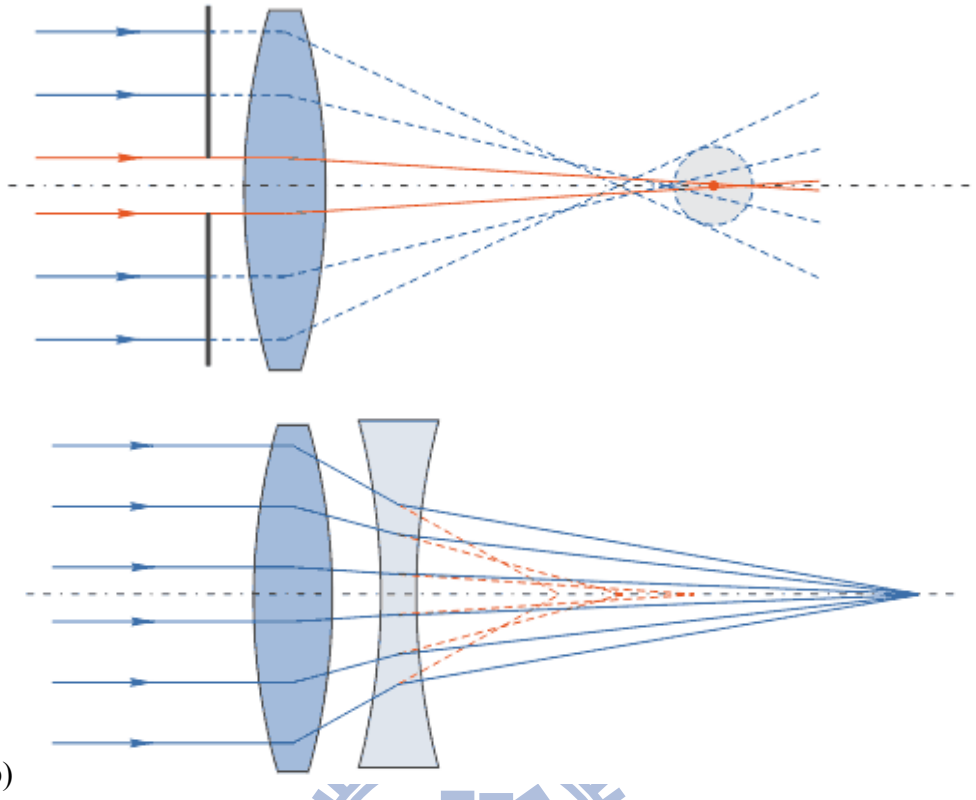

Figure 1.3 (a) Schema of the spherical aberration in a spherical lens (b) Lens group for eliminating spherical aberration [3].

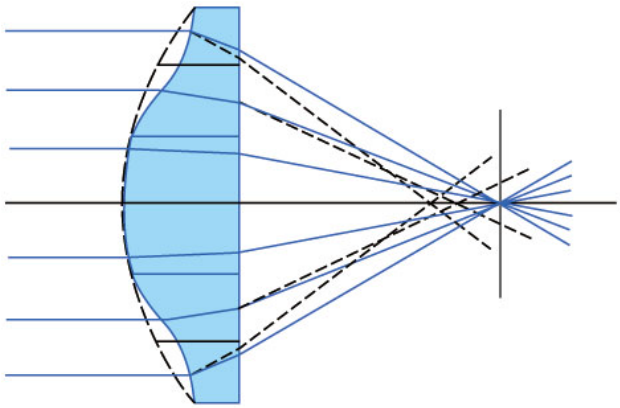

Figure 1.4 Aspherical lens focusing the collimating lights on a single point of the lens axis [4].

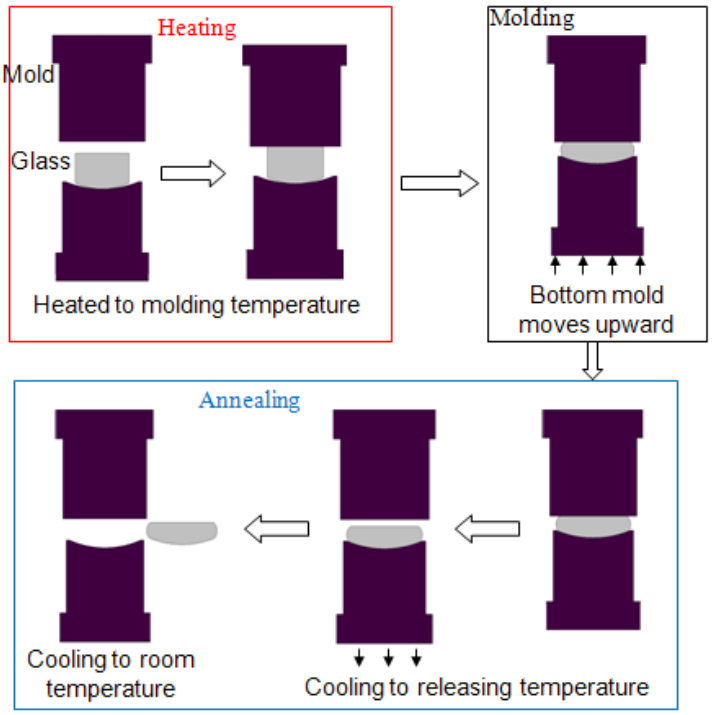

Figure 1.5 Schema of the optical glass molding process.

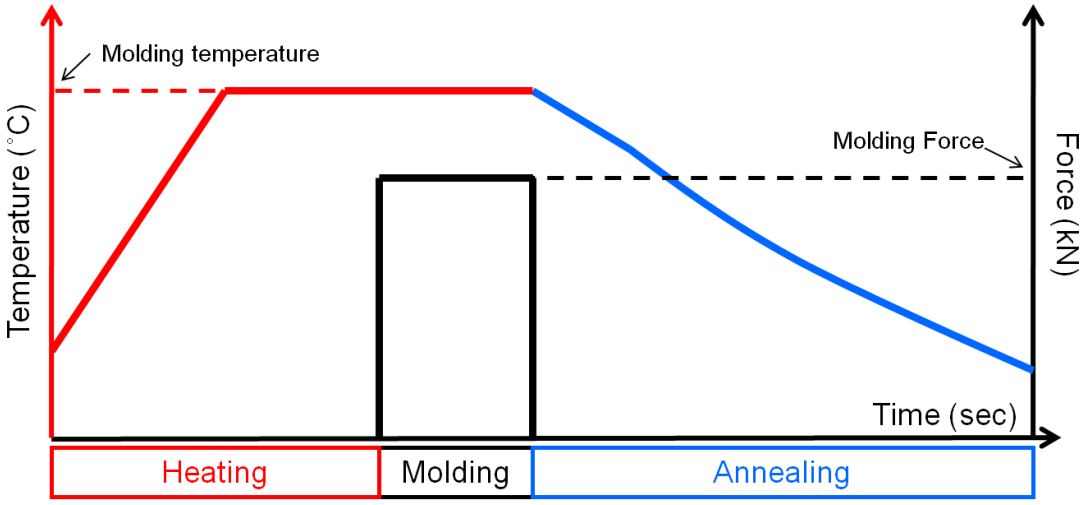

Figure 1.6 Schema of the optical glass molding history

Figure 1.7 Various optical lenses (Bi-convex lens, Bi-concave lens, Ball lens, Meniscus lens, Insertion lens, f-θ lens, Micro lens array, Fiber array) fabricated by optical glass molding technology (Toshiba Machine Co.) [6].

CHAPTER 2 MATERIAL MODELS OF OPTICAL GLASSES

Before investigating the optical glass material models used in the glass molding process, section 2.1 provides a basic understanding of the viscosity of the glass, which represents the mechanical behavior of the glass corresponding to a wide range of temperatures from room temperature to the glass melting temperature. Also, because the thermal history of the molding process passes through the glass transition region, the behaviors of the optical glass in this region (viscoelastic and structural relaxation) are introduced in section 2.2. For the optical glass material models used in the FEA on the glass molding process (thermal expansion, Newtonian fluid, stress and structural relaxation), section 2.3 introduces them respectively corresponding to each forming stages.

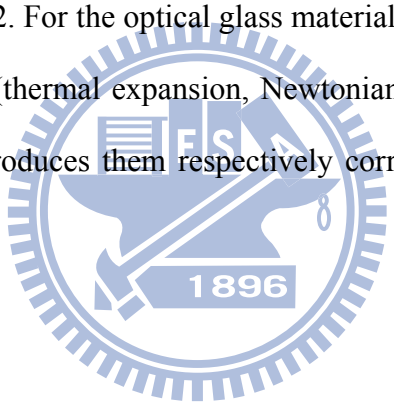

2.1 Viscosity

The viscosity plays an important role in determining various processing conditions in forming such as: melting, casting, drawing, and pressing. In addition to controlling the glass formation, viscosity is also very important in determining the temperature of annealing to remove internal stresses. The viscosity of optical glass depends on its composition and is a function of temperature.

Viscosity is defined as the ratio between shearing force and rate of flow. If two planes of area A at a distance d are displaced against each other at a relative velocity v by a force F, the viscosity η is [19]:

$$\eta = \frac{Fd}{Av} \tag{2.1}$$

The original unit Poise (P), which is given in dyne·s·cm^{-2}, is often used in prior

literatures and the glass industry. The SI unit of viscosity is Pa·s; 1 Pa·s = 10 P.

Figure 2.1 shows a typical curve for viscosity as a function of temperature for a commercial soda-lime-silicate glass. Formation of a glass object typically starts from a glass melt at extremely high temperature, usually above 1000°C. As the glass cools to a temperature that the glass melt is fluid enough to be formed by pressing or drawing, but viscous enough to retain its shape after forming, this temperature is designated as the *working point*, at which its viscosity is 10^3 Pa·s. Once initial shape was formed, the glass object is supported until the viscosity reaches a value sufficient high to prevent further deformation of the glass under its own weight. This temperature point is the *softening point* (SP) and the corresponding viscosity is $10^{6.65}$ Pa·s. In a glass forming process, the internal stresses which result from cooling are usually reduced by annealing. The *annealing point* (AP) corresponds to the maximum temperature in the annealing range at which the internal stresses of glass will be substantially eliminated. Viscosity of the glass is 10^{12} Pa·s at this point. The *strain point* (StP) corresponds to the lowest temperature in the annealing range at which viscous flow of glass will not occur. Viscosity of the glass is $10^{13.5}$ Pa·s at this point.

The other two glass reference points are determined from the measurements of thermal expansion curve of a glass and are often marked for forming reference (as shown in Figure 2.3). They do not correspond to exact viscosities. The *glass transition temperature* (T_g) is determined as the intersecting point of the slopes of the glassy and liquid states. The viscosity corresponding to T_g for common glasses has an average value of $10^{11.3}$ Pa·s. The *yield point* (At) is designated as the maximum measured value on the thermal expansion curve. The viscosity corresponding to At lies in the range between 10^8 to 10^9 Pa·s.

Arrhenius equation and Vogel-Fulcher-Tamman (VFT) equation are commonly used to describe the temperature dependence of viscosity for glass. The expression for the

Arrhenius equation is given by [21]:

$$\eta = \eta_0 \exp\left(\frac{\Delta H}{RT}\right) \tag{2.2}$$

where η_0 is a temperature-independent coefficient called the pre-exponential factor, ΔH is the activation energy for viscous flow, R is a gas constant and T is the current temperature. The Arrhenius equation provides a good fit in the transformation temperature range (10^{13} to 10^{9} Pa·s) and at high temperatures where the glass behaves like a fluid. A relatively good fit over the entire temperature range is the VFT equation [22]:

$$\log \eta(T) = A + \frac{B}{(T - T_0)} \tag{2.3}$$

, where A, B and T_0 are the fitting constants that can be obtained from the above mentioned reference temperatures. For the optical glass used in this study, L-BAL42, A=-31.85, B=37418.30°C, and T_0=-340.30°C and the fitted viscosity curve is shown in Figure 2.2.

Common glass viscosity measuring methods are: Rotation viscometer, used in $10^{3.5}$–10^{9} Pa·s range; Falling sphere viscometer, used in 1–10^{6} Pa·s range; Fiber elongation viscometer, used in 10^{5}–10^{12} Pa·s range; Beam-bending viscometer, used in 10^{8}–10^{13} Pa·s range; Parallel plate, viscometer used in 10^{5}–10^{8} Pa·s range; Penetration viscometer, used in 10^{8}–10^{12} Pa·s range and torsion viscometer, used in 10^{11}–10^{14} Pa·s range.

2.2 Behaviors in Glass Transition Region

2.2.1 Viscoelastic

While applying a load on the glass in the liquid state, low viscosity makes it behave as a viscous flow. When a load applies on the glass in the glassy state, high viscosity makes it exhibit elastic response as ordinary solids. In the glass transition region, the intermediate region between liquid and glassy state, the response of glass subjected to

the applied load exhibits both fluid and solid like behavior, and this is termed as the *viscoelastic* behavior.

The viscoelastic behavior can be represented by different combinations of springs and dashpots to describe the relationship between stress and strain in the material. As shown in Figure 2.4. Spring represents the time-independent elastic deformation and the dashpot represents the time-dependent viscous flow, related to the strain rate. The Maxwell model, in which the elastic and viscous elements are connected in series, is often used to describe the response to a constant strain (i.e. stress relaxation). The Kevin-Voigt model, in which the elastic and viscous elements are connected in parallel, is often used to describe the response to a constant stress (i.e. creep). The responses of each model are shown in Figure 2.5 and Figure 2.6.

In the Maxwell model, as shown in Figure 2.4a, the spring represents Hookean elastic behavior, so the strain in the spring is $\varepsilon_{12}^{E} = \sigma_{12}/2G$, where G is the shear modulus. The dashpot represents Newtonian viscous behavior and the strain rate in the dashpot is $\dot{\varepsilon}_{12}^{V} = \sigma_{12}/2\eta$, where η is the viscosity. The total strain is $\varepsilon_{12} = \varepsilon_{12}^{E} + \varepsilon_{12}^{V}$ and the relation between strain rate and the stress is described as [21]:

$$\dot{\varepsilon}_{12} = \dot{\varepsilon}_{12}^{E} + \dot{\varepsilon}_{12}^{V} = \frac{\dot{\sigma}_{12}}{2G} + \frac{\sigma_{12}}{2\eta} \tag{2.4}$$

By integrating and solving the equation, the time dependent stress is obtained as:

$$\sigma_{12}(t) = 2G\left[\varepsilon_{12}(0)\varepsilon^{-t/\tau_s} + \int_0^t \dot{\varepsilon}_{12}\varepsilon^{-(t-t')/\tau_s}dt'\right] \tag{2.5}$$

where τ_s is called the stress relaxation time and is given by η/G.

If the strain is constant ($\dot{\varepsilon}_{12} = 0$), equation (2.5) reduces to:

$$\sigma_{12}(t) = \sigma_{12}(0)\varepsilon^{-t/\tau_s} \tag{2.6}$$

Thus the Maxwell model shows simple exponential decay of the stress.

In the Kevin-Voigt model, the strain is the same in each element, but the stress is σ_{12}^{E} in the spring and σ_{12}^{V} in the dashpot. The total stress is:

$$\sigma_{12} = \sigma_{12}^{E} + \sigma_{12}^{V} = 2G\varepsilon_{12} + 2\eta\dot{\varepsilon}_{12} \tag{2.7}$$

and the time dependent strain is given by:

$$\varepsilon_{12}(t) = \frac{1}{2\eta}\int_{o}^{t} \sigma_{12}\varepsilon^{-(t-t')/\lambda_s} dt' \tag{2.8}$$

If the stress is constant, equation (2.8) reduces to:

$$\varepsilon_{12}(t) = \frac{\sigma_{12}}{2G}(1-\varepsilon^{-t/\lambda_s}) \tag{2.9}$$

which represents delayed elasticity, which is neither an instantaneous elastic nor a viscous flow. λ_s is called the retardation time in this creep equation.

2.2.2 **Structural relaxation**

When glass cools from liquid state, an instantaneous decrease in interatomic spacing and a time-dependent rearrangement of constituent atoms occur simultaneously. At the liquid state, high temperature and low viscosity provide the atoms with high energy and large spaces to rearrange and let rearrangement keep up with the instantaneous decrease in interatomic spacing. As glass cools through the glass transition region, lower temperature and higher viscosity make the rearrangement of constituent atoms lag behind decrease in interatomic spacing. As cooling continues, the viscosity becomes so large that rearrangement of the constituent atoms ceases and only interatomic spacing decreasing continues. In this case, the structure can be treated as frozen in a fixed configuration, known as the glassy state.

The region from where the arrangement of constituent atoms cannot synchronize with the decrease in interatomic spacing, to the ceasing of rearrangement, is termed as the *glass transition region*. When glass cools through the glass transition region with a

slow cooling rate, the final structure will be denser than the glass with fast cooling rate because the time is sufficient for atoms to rearrange. This time-dependent characteristic of structural change in the presence of a temperature change in the transition region is called *structural relaxation*. Figure 2.7 shows the structural relaxation phenomenon. Detailed descriptions on the mathematical model of the structural relaxation are in subsection 2.3.3.

2.3 Glass Material Models for FEA on Glass Molding Process

The molding process defines both the lens final shape and the residual stress inside the lens which govern the optical performances of the lens. Detailed glass material properties must be considered into the FEA. These inputted material properties are described in the following sections corresponding to each processing stages.

2.3.1 Heating Stage

The heating stage comprises heating the glass to the molding temperature, and keeping the molding temperature for a period of time to let the glass, the molds and the environment achieve isothermal state. Figure 2.8 shows the thermal and loading history of the heating stage.

Thermal expansion is a major factor affecting deformation in the heating stage. As the temperature increases, the glass expands, and the coefficient of thermal expansion changes accordingly. For the expansion property, glass manufacturers usually only provide a constant coefficient of thermal expansion below T_g. As for the coefficients of thermal expansion above T_g, Jain [2], Chen et al. [17], and Yan et al. [24] attempted to use values calculated by a simplified empirical assumption (i.e. $\alpha_l = 3\alpha_g$). To accurately predict the shape of the formed lens, we conducted a thermal expansion experiment to obtain the actual coefficient of thermal expansion, and subsequently introduced this

coefficient into FEA.

2.3.2 **Molding Stage**

Followed by the heating stage, the glass is molded at a fixed molding temperature (which is usually set at 30°C above At where viscosity is around 10^8 Pa·s) with a constant molding force in the subsequent molding stage. Figure 2.9 shows the thermal and loading history of the molding stage.

Due to low viscosity at the molding temperature, glass can be modeled as a Newtonian fluid when subjected to an applied force during the molding stage. The mathematical model of Newtonian fluid can be illustrated by

$$\sigma = 3\eta(T)\dot{\varepsilon} \tag{2.10}$$

where σ is the effective stress, $\dot{\varepsilon}$ is the effective strain rate, and $\eta(T)$ is the temperature-dependent viscosity. The corresponding viscosity at any given temperature above T_g can be calculated by fitting standard reference points with the VFT equation (eq. (2.3)).

2.3.3 **Annealing Stage**

In the annealing stage, the applied molding force is released and the glass lens is cooled form the molding temperature. Cooling rates were controlled by the nitrogen flow rate. Figure 2.10 shows the thermal and loading history of the annealing stage. Structural relaxation, stress relaxation and coefficients of thermal expansion are the major factors governing the FE model in this stage.

In the annealing stage, because of the time-dependent characteristic of structural change in the presence of a temperature change, structural relaxation property must first be included in FEA to calculate the amount of shrinkage.

To analyze the structural relaxation property, Tool [25] introduced a fictive

temperature, T_f, to represent the actual temperature at which a particular structure would be fully relaxed to the liquid state (achieved equilibrium configuration) after a long time (as Figure 2.11 shows).

While glass cools through the transition region, the response to a step change in temperature from T_1 to T_2 can be described by [21]:

$$\frac{p(T_2,t)-p(T_2,\infty)}{p(T_2,0)-p(T_2,\infty)}=M_p(t)=\frac{T_f(t)-T_2}{T_1-T_2} \tag{2.11}$$

where 0 and∞ respec tively represent the instantaneous and long-term values of property (p) following a temperature change. T_f is the fictive temperature, which is defined so that the quantity on the right-hand side of the equation is the unrelaxed fraction at time t. When t=0, the structure has not yet started to relax, thus $T_f(0)$ is T_1. As time increases, the actual temperature at which the structure has already relaxed to liquid state will become increasingly closer to T_2. When the structure has sufficient time to fully relax (t=∞), $T_f(\infty)=T_2$. The response function can then be described by [26]:

$$M_p(t)=\exp[-(t/\tau_p)^{\beta}] \tag{2.12}$$

where β is a constant between 0 and 1, and τ_p is the structural relaxation time.

When the relaxation curves are plotted with log (time) as the abscissa, they shift toward shorter time scales without changing shape as the temperature increases (as Figure 2.12 shows). This behavior, called thermorheological simplicity, makes it possible to use relaxation times, $\tau_{p,ref}$, evaluated at a suitable reference temperature, T_{ref}, and incorporate the temperature dependence in a new variable, the reduced time, ξ [26]:

$$\xi=\int_0^t\frac{\tau_{p,ref}}{\tau(T(t'))}dt' \tag{2.13}$$

The concept of reduced time, ξ, is introduced in the spirit of thermorheological simplicity materials to capture the disparate nonlinear response curves on a single

master curve. Hence,

$$M_p(\xi) = \exp[-(\xi / \tau_{p,ref})^{\beta}] \tag{2.14}$$

Because the relaxation time, τ_P, depends not only on temperature but also on thermal history, Narayanaswamy [27] proposed the following equation to calculate τ_P:

$$\frac{\tau_p}{\tau_{p,ref}} = \exp\left\{-\frac{\Delta H}{R}\left[\frac{1}{T_{ref}} - \frac{x}{T} - \frac{(1-x)}{T_f}\right]\right\} \tag{2.15}$$

and the fictive temperature, T_f:

$$T_f(t) = T(t) - \int_0^t M_p(\xi(t) - \xi(t')\frac{dT(t')}{dt'}dt' \tag{2.16}$$

where ΔH is the activation energy, R is the ideal gas constant and x is a fraction parameter with a value between 0 and 1.

Once the fictive temperature is known, the volume change of glass can be represented by the derivative of the property with respect to temperature [26]:

$$\frac{1}{V(0)}\frac{dV(T)}{dT} = \alpha_{vg}(T) + \left[\alpha_{vl}(T_f) - \alpha_{vg}(T_f)\right]\left(\frac{dT_f}{dT}\right) \tag{2.17}$$

where $V(0)$ is the initial volume, α_{vl} and α_{vg} are the volumetric thermal contraction coefficients of the liquid and glass respectively. In the FEA, α_{vl} and α_{vg} are calculated automatically from the input of the obtained linear coefficients of thermal expansion in the liquid state and glassy states respectively. The linear thermal strain induced from the structural relaxation behavior can then be calculated in FEA by:

$$\varepsilon^{th} = \frac{1}{3}\frac{\Delta V}{V(0)} \tag{2.18}$$

Owing to the induced linear thermal strains in the annealing stage, the corresponding stresses will occur.

Because the thermal history of the glass in the annealing stage passes through the glass transition region, which is an intermediate state between liquid and solid where glass behaves as a viscoelastic material, stresses induced from thermal strains will

have the ability to relax to an extent according to the cooling rate and the unreleased stresses finally will form the residual stresses. To calculate the residual stress, stress relaxation property is also introduced into FEA in the annealing stage.

A generalized Maxwell model was used to model the stress relaxation in the glass transition region. This Maxwell model consists of a series of springs with shear modulus G_i and dashpots with viscosity η_i (as Figure 2.13 shows). The stress relaxation modulus $G(t)$ and the stress relaxation function $\psi(t)$ for this parallel model can be represented by:

$$G(t) = 2G\sum_{i=1}^{n} w_i \exp(-t/\tau_{si}) \tag{2.19}$$

$$\psi(t) = \frac{G(t)}{G(0)} = \sum_{i=1}^{n} w_i \exp(-t/\tau_{si}) \tag{2.20}$$

At time t=0, $G(0)$=2G, τ_{si} are the stress relaxation times calculated by η_i/G_i, and w_i represent the corresponding weighing factors, obtained by fitting to the stress relaxation experimental data. This stress relaxation property can be obtained from a stress relaxation experiment (will be discussed in chapter 3) and subsequently be introduced into FEA.

2.4 Summary

From the introduction on the viscosity of the glass corresponding to a wide temperature range, to the viscoelastic and structural relaxation behaviors of the glass in the glass transition region, basic understandings of the mechanical behaviors of the glass were presented in this chapter. Moreover, material models i.e. coefficient of thermal expansion, Newtonian fluid, structural and stress relaxation properties for the FE model are introduced respectively corresponding to the heating, molding and annealing stages in this chapter. The following chapter will describe the material property experiments on completing these material models.

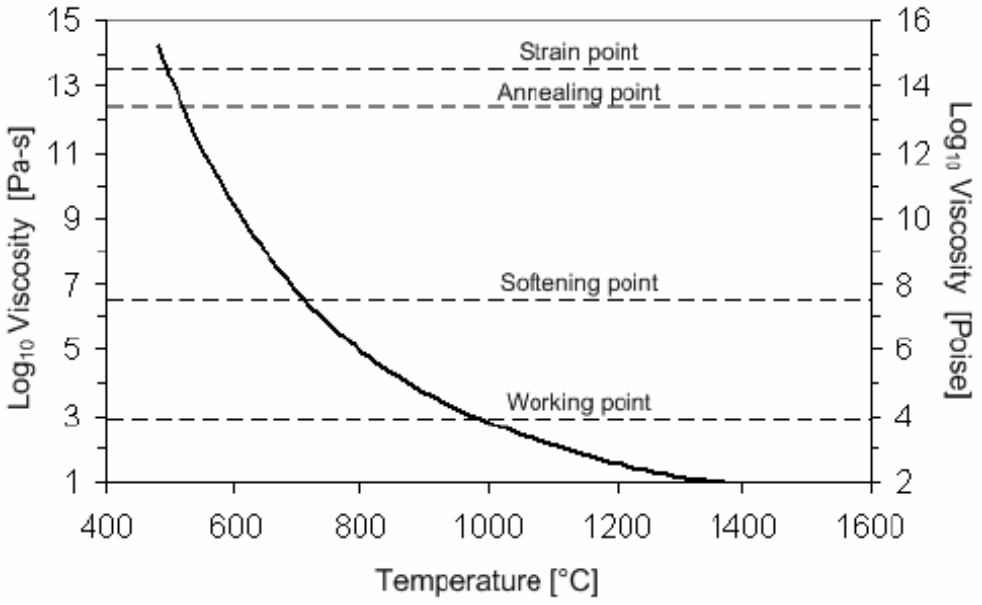

Figure 2.1 Typical curve for viscosity as a function of temperature for a commercial soda-lime-silicate glass [19].

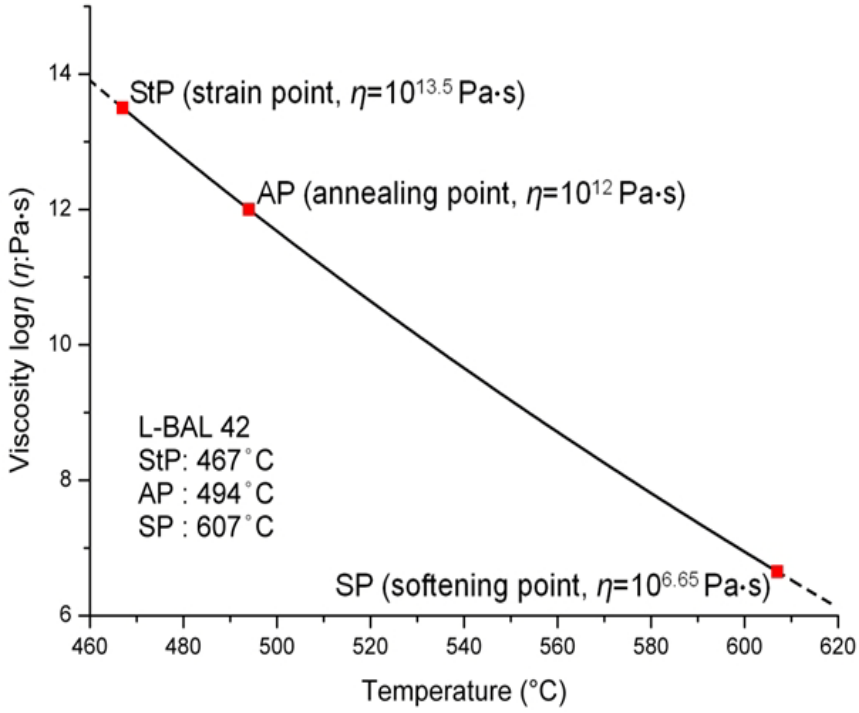

Figure 2.2 Standard points of L-BAL42 and the fitted viscosity curve (by VFT equation).

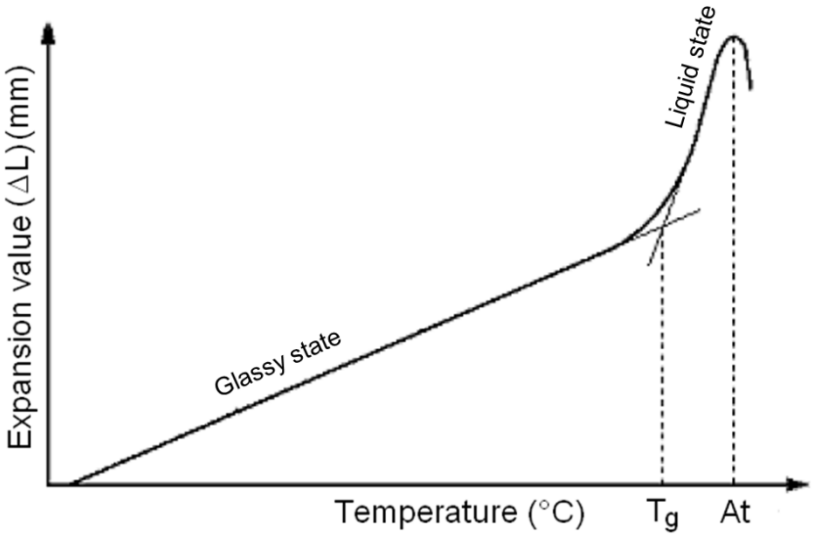

Figure 2.3 Thermal expansion curve of a typical optical glass [20].

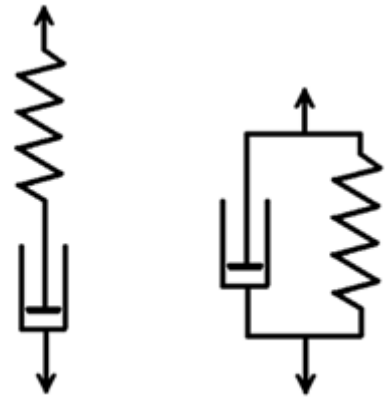

(a) (b)

Figure 2.4 Commonly used viscoelastic models (a) Maxwell model (b) Kevin-Voigt model.

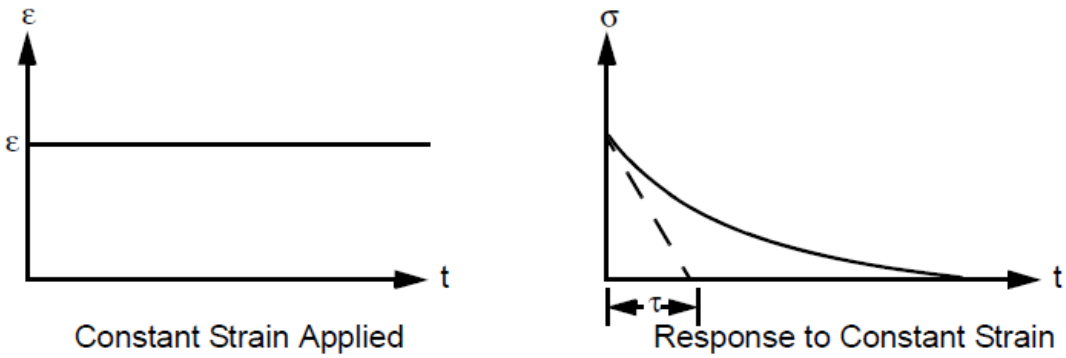

Figure 2.5 Stress response to applied constant strain (Maxwell model) [21].

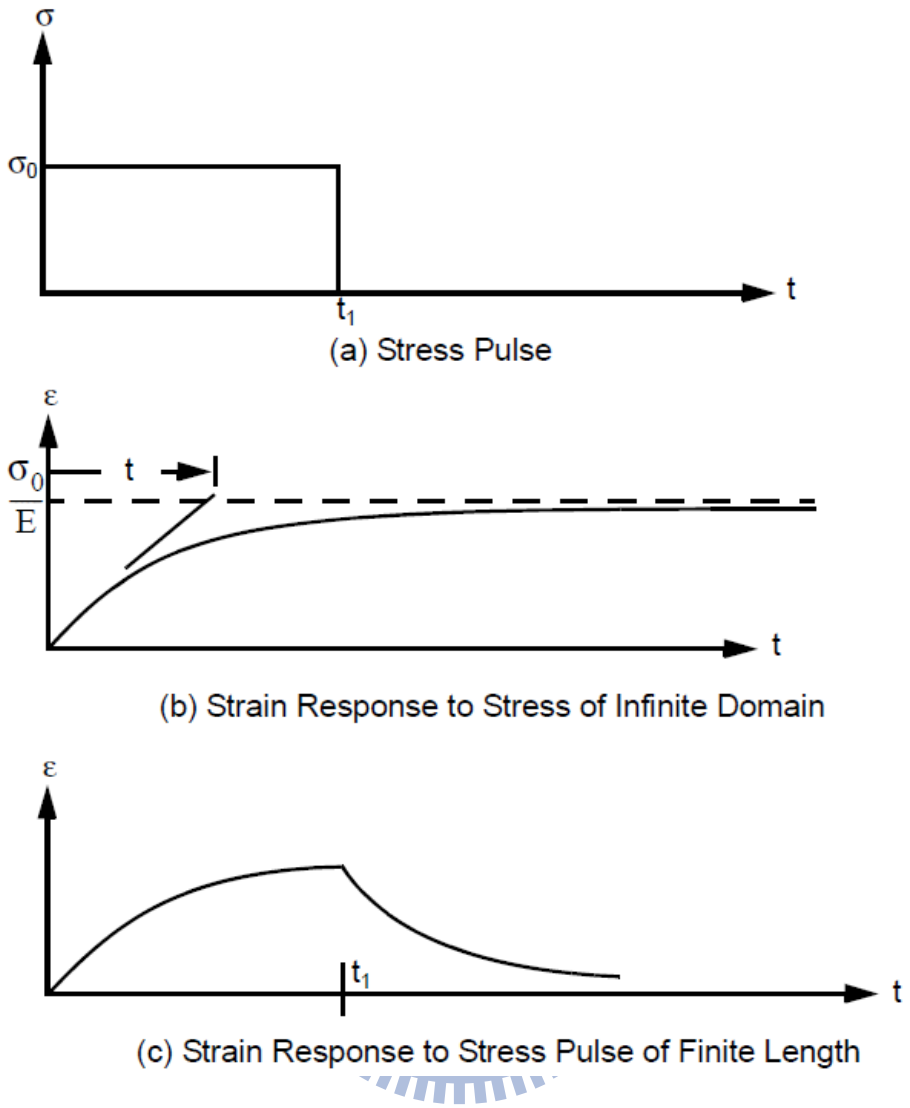

Figure 2.6 Strain response to applied stress (Kevin model) [23]

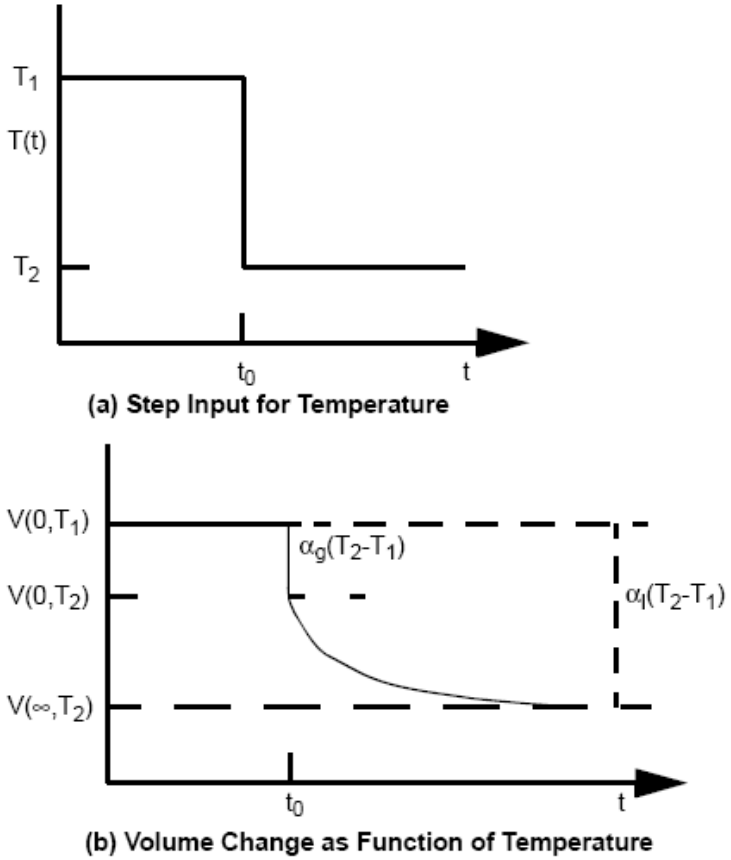

Figure 2.7 Structural relaxation phenomenon [23].

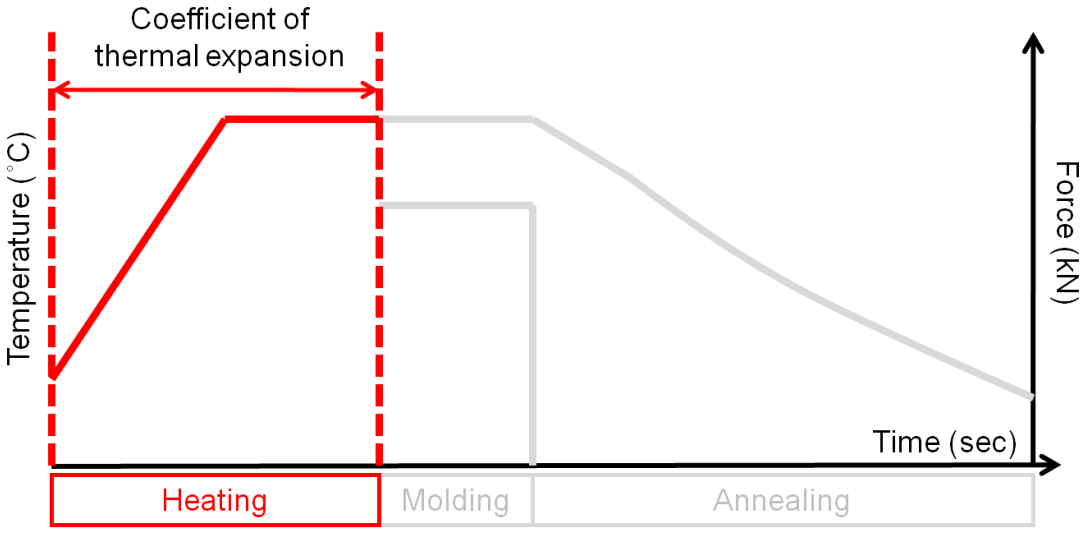

Figure 2.8 Optical glass material properties for the FEA in the heating stage.

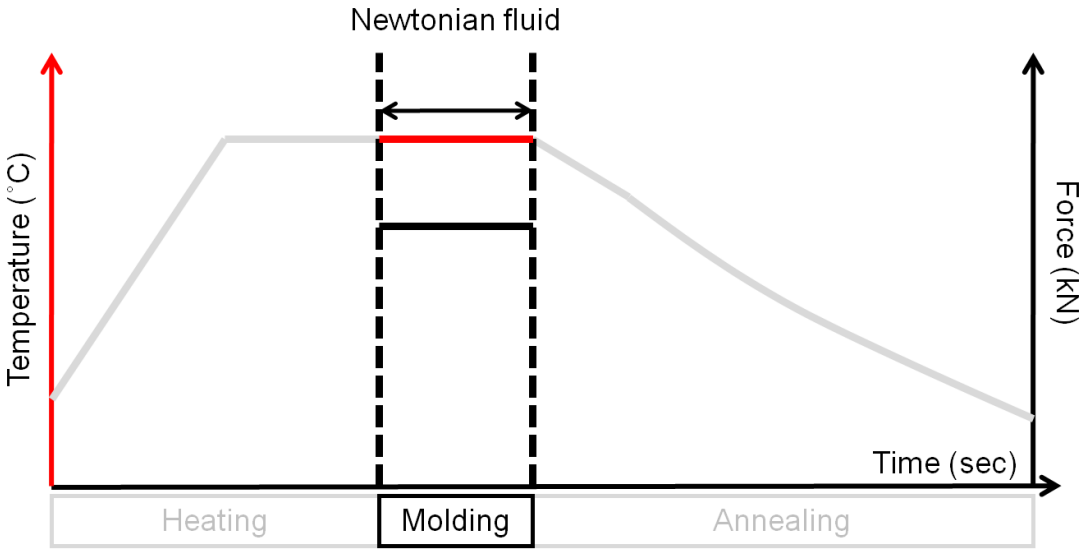

Figure 2.9 Optical glass material properties for the FEA in the molding stage.

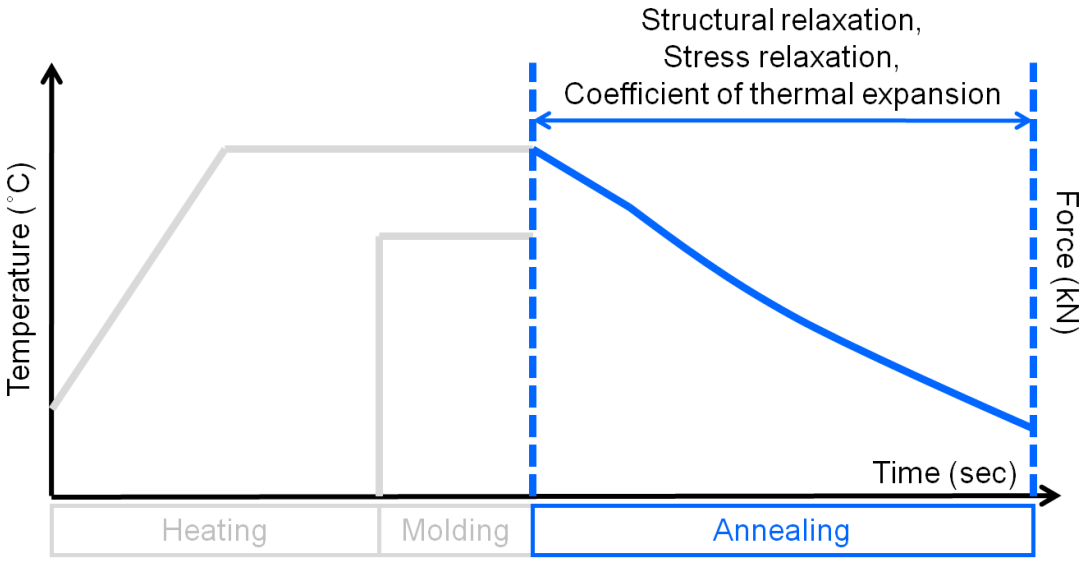

Figure 2.10 Optical glass material properties for the FEA in the annealing stage.

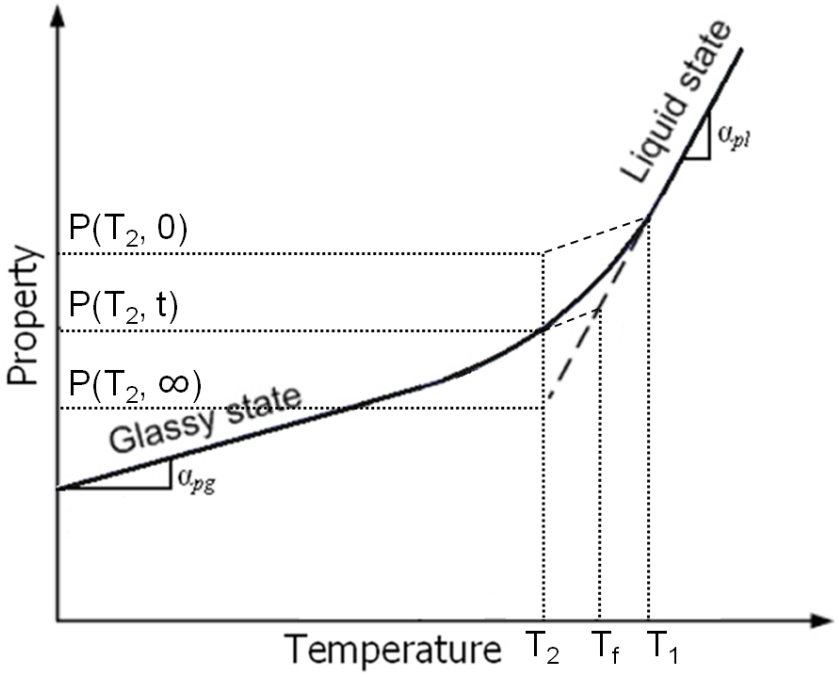

Figure 2.11 Property changes during the cooling of the glass-forming liquid.

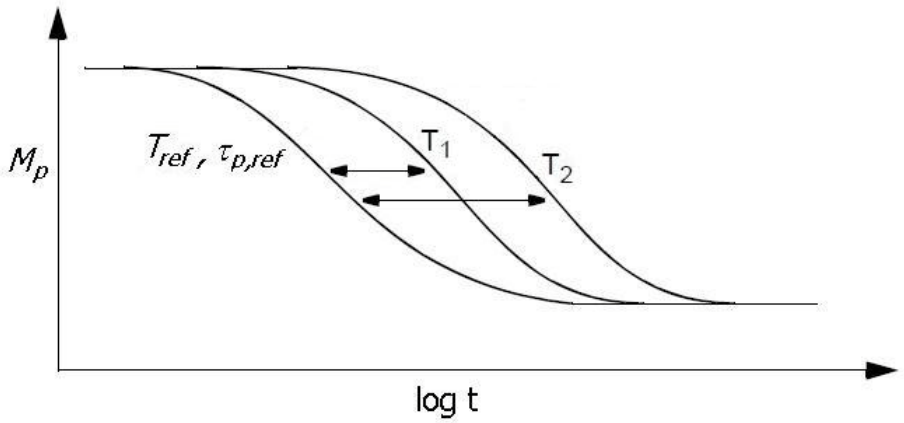

Figure 2.12 Relaxation curves exhibit thermorheological simplicity behavior at various temperatures (T_{ref}>T_1>T_2) with a reference temperature T_{ref} and evaluated $\tau_{p,ref}$.

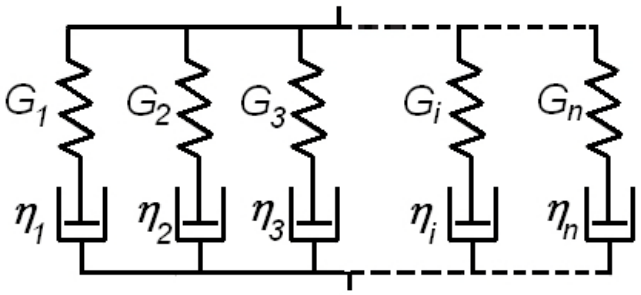

Figure 2.13 Generalized Maxwell model for modeling viscoelastic stress relaxation behavior.

CHAPTER 3 MATERIAL PROPERTY EXPERIMENTS

In order to obtain detailed optical glass material properties for constructing the FE model of the glass molding process, this study performed three kinds of material experiments. The thermal expansion coefficients, structural relaxation property and stress relaxation property were obtained by dilatometric measurement, DSC measurement and uniaxial stress relaxation experiment respectively. Detailed descriptions are presented in the following sections.

3.1 Thermal Expansion Experiment

For the expansion property, glass manufacturers usually only provide the coefficient of thermal expansion below T_g. Scholze [28] indicated that the thermal expansion coefficient above T_g (α_l) is about three times larger than that under T_g (α_g) based on the relationship between the volumetric change and the Poisson's ratio. Chen et al. [17] and Yan et al. [24] directly introduced this simplified assumption into FEA on the glass molding process. Jain [2] preformed experiment to measure the thermal expansion coefficient of BK7 glass (Schott Co.). The measured α_l is 3.77×10^{-5}/°C which is over four times larger than its α_g (8.3×10^{-6}/°C**).** Hence the simplified assumption cannot accurately describe the expansion coefficient above T_g. Thermal expansion experiment should be performed.

To obtain the detailed thermal expansion behavior of L-BAL42 from room temperature to molding temperature, this study performed a thermal expansion experiment using a dilatometer, Netzsch DIL 402C (Netzsch Co.), as Figure 3.1 shows. It is capable to heat the glass samples up to 1600°C**.** A standard cylindrical specimen with 25mm in length and 8mm in diameter was used**.** The experimental temperature

was controlled to be raised at a rate of 2°C/min in the low temperature range (25°C to 100°C), and 4°C/min in the high temperature range (100°C to 580°C).

Figure 3.2 shows the thermal expansion experimental results, where α_g= 9.12×10^{-6}/°C and α_l =9.17×10^{-5}/°C. The expansion curve rapidly drops when the temperature reaches At (538°C). This is because after At, the glass continues to dilate, but it is too soft to prevent the probes at both ends of the specimen from sinking into the glass. However, the linear coefficient of thermal expansion for the liquid state can still be obtained from the maximum slope within the region between T_g and At.

The linear coefficient of thermal expansion for the solid state was obtained by linear fitting to the measured results from 100°C to 300°C. The linear coefficient of thermal expansion obtained for the glassy state differs slightly from the manufacturer-given value (8.8×10^{-6}/°C). The difference may be due to slight variations in composition between each batch of glass. This small difference (2.8×10^{-7}/°C) will not significantly affect the expanded quantity of the glass preform. But, owing to the lacking thermal expansion coefficient for the liquid state from the manufacturer, thermal expansion experiments should still be performed.

3.2 Structural Relaxation Experiment

Scherer [21], Webb et al, [29] and Sipp et al. [30] mentioned that the relaxation properties in volume, enthalpy, specific heat, and other material properties are equivalent with respect to structural relaxation property. Usually, volume relaxation properties are measured using dilatometer and will take hours to days to obtain the results. Moynihan et al. [31],[32] and DeBolt et al. [33] successfully obtained the structural relaxation property by using differential scanning calorimetry (DSC) to measure specific heat variation in the glass transition region with a constant heating rate and several different cooling rates. The time for one period of measurement is less

than an hour. DSC largely improves the convenience for exploring structural relaxation property of the glasses.

The DSC directly measures the heat capacity C_p (equal to dH/dT), where H is the enthalpy. Appendix A provides detailed descriptions on the DSC measurement. Figure 3.3 shows the schema of the temperature dependence of H and C_p during fast and slow cooling.

According to Moynihan et al. [31], the fictive temperature is defined by:

$$H(T) = H_e(T_f) - \int_T^{T_f} C_{pg} dT' \tag{3.1}$$

where H_e is the equilibrium enthalpy and C_{pg} is the heat capacity of the glass. Since

$$H(T) = H_e(T_0) - \int_{T_0}^{T} C_p dT' \tag{3.2}$$

and

$$H_e(T_f) = H_e(T_0) - \int_{T_0}^{T_f} C_{pl} dT' \tag{3.3}$$

Equation (3.1) can be written as:

$$\int_{T_0}^{T_f} (C_{pl} - C_{pg}) dT' = \int_{T_0}^{T} (C_p - C_{pg}) dT' \tag{3.4}$$

Where C_{pl} is the heat capacity of the liquid (equilibrium state) and T_0 is the initial temperature, which is above the transition region. Equation (3.4) can be used to obtain $T_f(T)$ from the heat capacity data. Taking the derivative of eq. (3.4) with respect to T leads to:

$$\frac{dT_f}{dT}(T) = \frac{C_p(T) - C_{pg}(T)}{C_{pl}(T_f) - C_{pg}(T_f)} \tag{3.5}$$

dT_f/dT approaches unity above the glass transition ($T_f = T$) and zero below the transition (T_f =T_g=constant).

According to the structural relaxation property, different thermal histories will cause different fictive temperatures T_f and different relaxation times τ_p. Along with the

equations proposed by Narayanaswamy [27], Hodge et al. [34] transformed these equations for numerical calculation as follows:

$$C_{p,n} = \frac{dT_f}{dT} = \frac{(T_{f,n} - T_{f,n-1})}{(T_n - T_{n-1})} \tag{3.6}$$

$$T_{f,n} = T_0 + \sum_{j=1}^{n} \Delta T_j \left\{ 1 - \left[\exp(-\sum_{k=j}^{n} \Delta T_k / q_k \tau_{0k})^{\beta} \right] \right\} \tag{3.7}$$

$$\tau_{0k} = A_0 \exp[\frac{x\Delta H}{RT_k} + \frac{(1-x)\Delta H}{RT_{f,k-1}}] \tag{3.8}$$

where $C_{p,n}$ is the normalized specific heat, q_k is the heating or cooling rate, β, A_0, x, and ΔH are the fitting parameters presenting different structural relaxation behavior of different materials.

This DSC experiment was conducted using Diamond DSC (PerkinElmer Inc.), as shown in Figure 3.4. The glass sample, L-BAL42, weights 33.3mg. The measurements were taken with 4 prior cooling rates on the sample (10, 24, 60 and 100°C/min) at temperatures ranging from 600°C to 400°C and heated over the same range at 10°C/min. The specific heat variations were normalized with the difference of the measured specific heat values between 600°C and 400°C (C_p(600°C)-C_p(400°C)), and then fitted by the above mentioned equations to obtain the fitting parameters.

Before fitting eq.(3.6) to eq.(3.8) with the DSC results, the ratio of $\Delta H/R$ can first be calculated based on the fact that viscosity obeys the Arrhenius equation (equation (2.2)). The slope of $\ln\eta$ versus $1/T$ is $\Delta H/R$, which this study calculates as 74091.33K. Figure 3.5 to Figure 3.8 shows the DSC results with the fitted curves. The best-fit parameters were A_0=1.1×10^{-39}, x=0.56 and β=0.69. The relaxation times τ_p were then obtained and introduced into FEA at a reference temperature of 600°C, at which the equilibrium state was achieved (where dT_f/dT equals 1). Table 3.1 shows the structural relaxation parameters used in the simulation during the annealing stage.

3.3 Stress Relaxation Experiment

FEA on the glass molding process at the annealing stage requires the shear stress relaxation property. However, the experimental apparatus with the ability to perform shear relaxation experiment at high temperature is difficult to acquire. Fortunately, via the relationship between the uniaxial (σ_{11}) and shear (σ_{12}) relaxation time [21]**:**

$$\sigma_{11} = \frac{3}{2(1+\nu)}\sigma_{12} \tag{3.9}$$

The shear stress relaxation property can be obtained by a uniaxial compressive stress relaxation experiment.

The uniaxial compressive stress relaxation experiment was performed using a furnace embedded material testing machine, as shown in Figure 3.9. Figure 3.10 shows the settings in the furnace. The temperature is raised by heating elements bedded inside the furnace and mold sets. With maximum load of 5kN and maximum temperature to 650℃**,** its ability is suitable for conducting experiments on the optical glasses. Cylindrical specimen with 8mm in length and 8mm in diameter was used in this experiment**.**

First attempt on the compressive stress relaxation experiment was conducted at the molding temperature of 568℃ (At+30℃). Figure 3.11 shows the experimental result. Obviously the stress relaxed too fast for the experimental apparatus to capture enough data points to accurately describe the relaxation curve.

Because the stress relaxation curves exhibit thermorheological simplicity behavior as well, the experiment was then performed at a lower temperature, 556°C (T_g+50℃) to obtain a more detailed stress relaxation curve.

Figure 3.12 presents the compressive uniaxial stress relaxation results. Although the stress still relaxed quite fast at this temperature (556°C, T_g+50°C), the experimental data captured with a 0.4sec interval is sufficient to grasp the shape of the relaxation

curve.

The experimental results were then fitted by a generalized Maxwell model and converted into shear relaxation properties by equation (3.9). Table 3.2 shows the weighing factors and the shear relaxation times.

3.4 Summary

The thermal expansion coefficients used in the heating and annealing stages of FEA were obtained by dilatometric measurement. Followed by DSC measurement on heat capacity, structural relaxation property was obtained from fitting the normalized measuring values with eq. (3.6) to eq. (3.8). The stress relaxation property were obtained by converting the uniaxial stress relaxation experimental results into shear ones by using eq. (3.9). These experimental obtained properties can then be inputted into FEA on the glass molding process. The verification on the FE model by experimental comparison is presented in the next chapter.

Figure 3.1 Dilatometer (DIL 402C, Netzsch) in the Center of EMO Materials and Nanotechnology, NTUT.

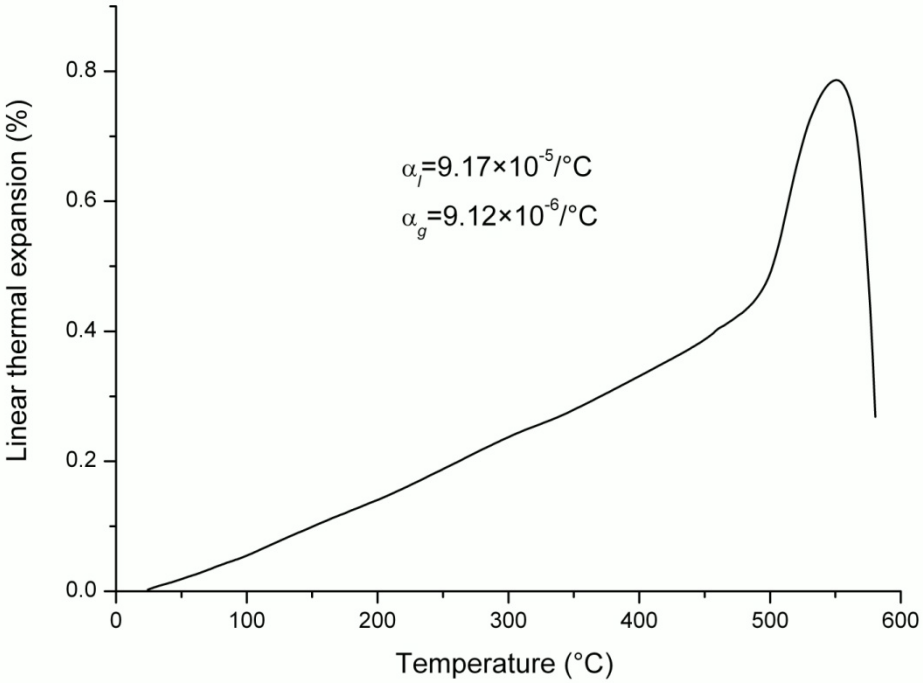

Figure 3.2 Measured linear thermal expansion curve (L-BAL42).

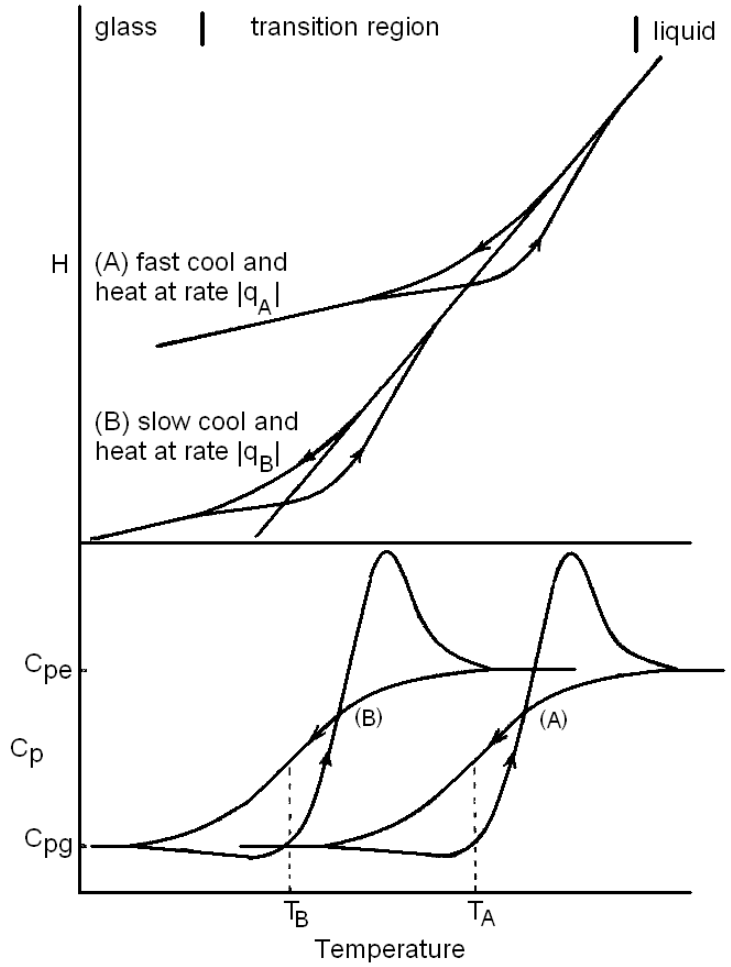

Figure 3.3 Enthalpy H and heat capacity C_p vs. temperature plots for a glass cooled and then reheated through the transition region at different rates q_A and q_B. Higher cooling rate $|q_A| > |q_B|$ causes higher fictive temperature $T_A > T_B$ [31].

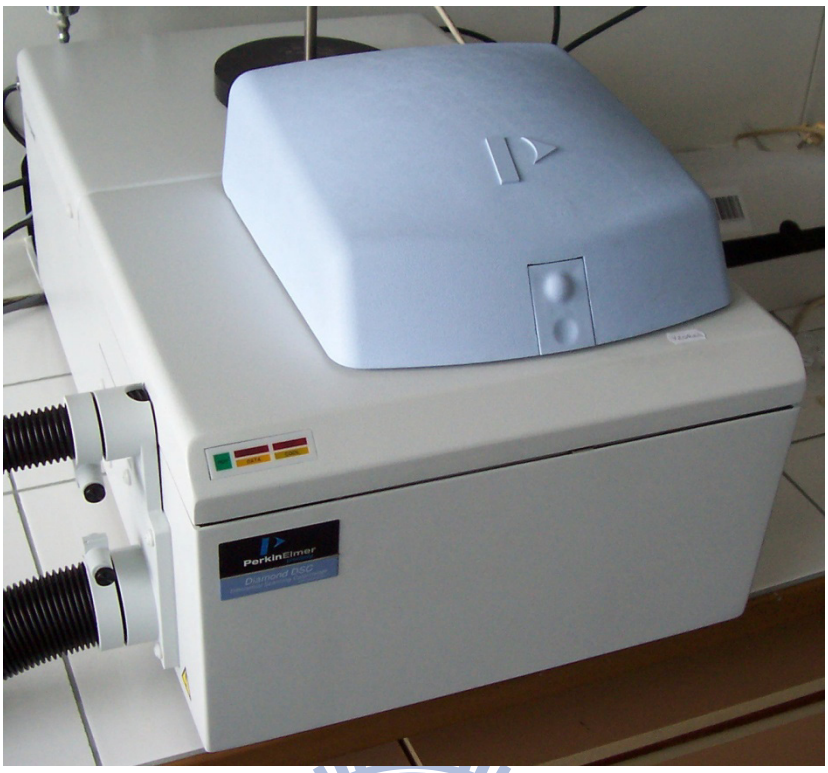

Figure 3.4 Differential scanning calorimeter (Diamond DSC, PerkinElmer Inc.) in the Department of Material Science and Engineering, NCTU.

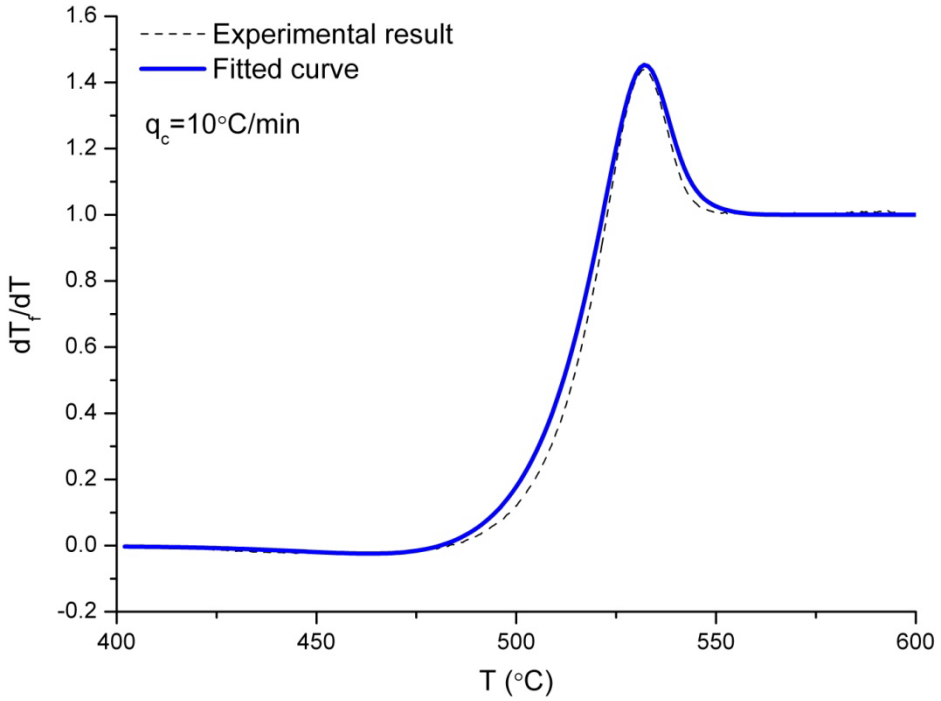

Figure 3.5 DSC fitting curve (prior cooling rate: 10°C/min).

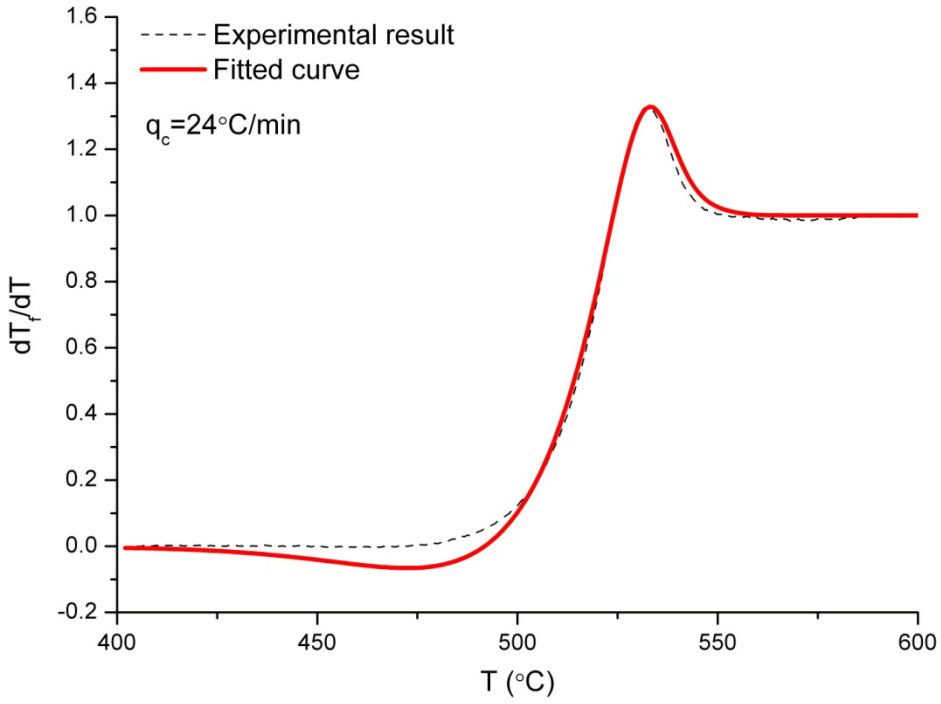

Figure 3.6 DSC fitting curve (prior cooling rate: 24°C/min).

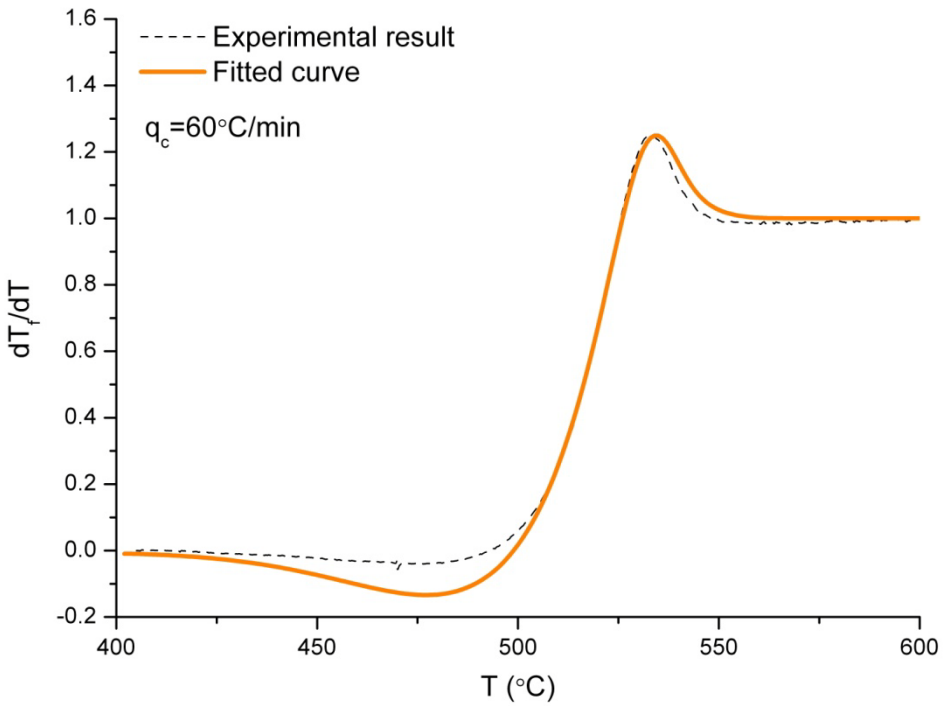

Figure 3.7 DSC fitting curve (prior cooling rate: 60°C/min).

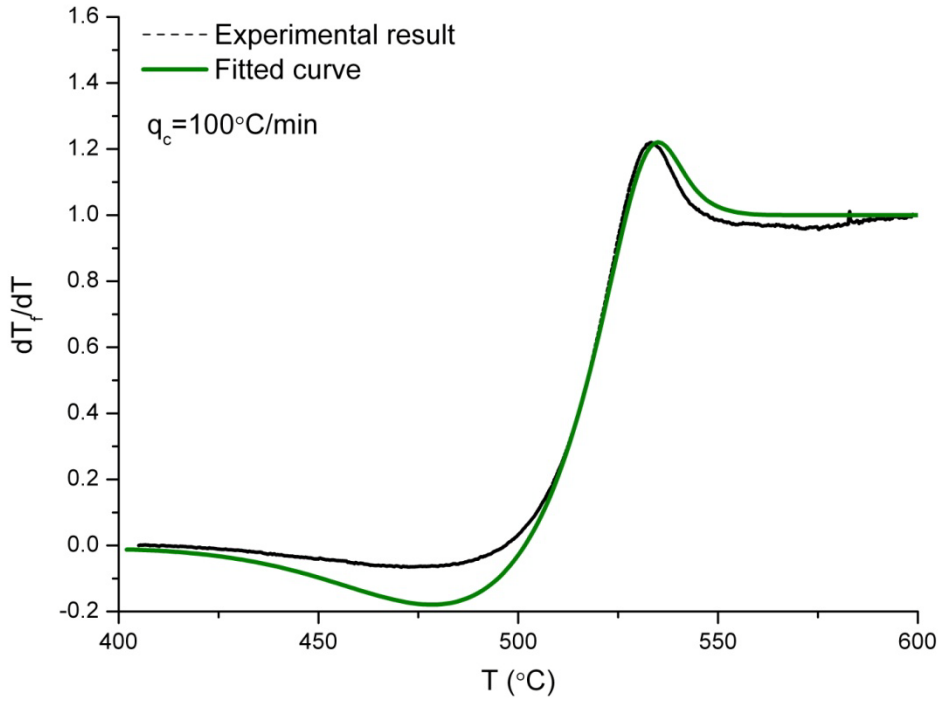

Figure 3.8 DSC fitting curve (prior cooling rate:1 00°C/min).

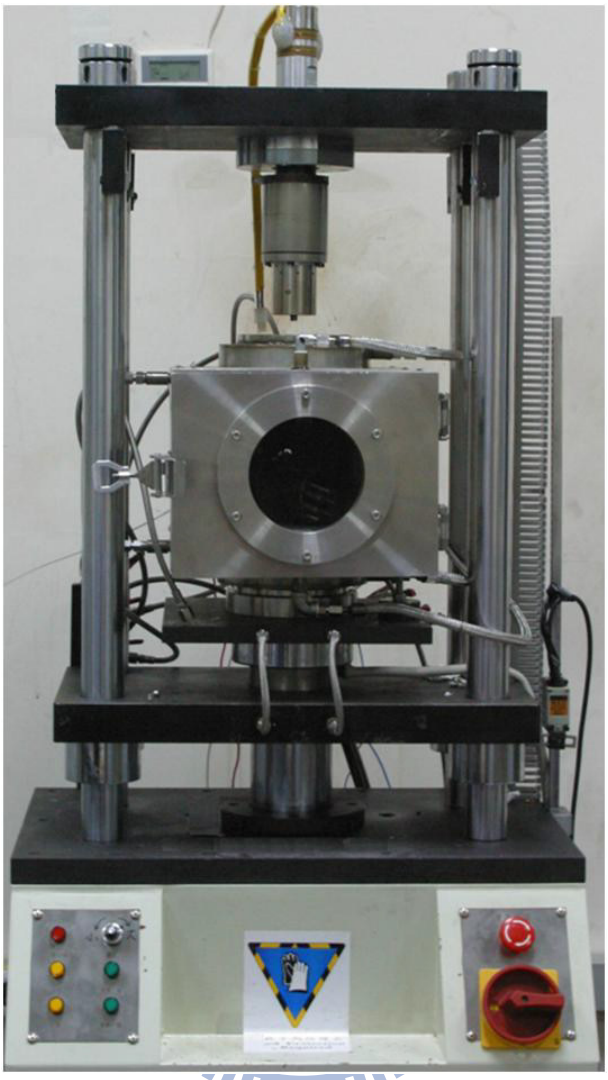

Figure 3.9 A furnace embedded material testing machine (designed by lab member, Jung-Chung Hung and assembled by Hungta Instrument Co.)

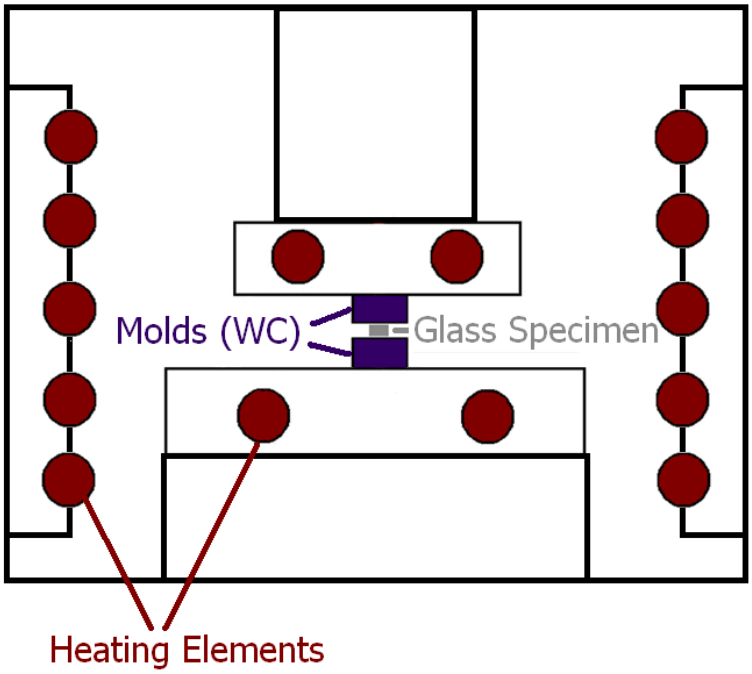

Figure 3.10 Settings in the furnace of the molding experiment.

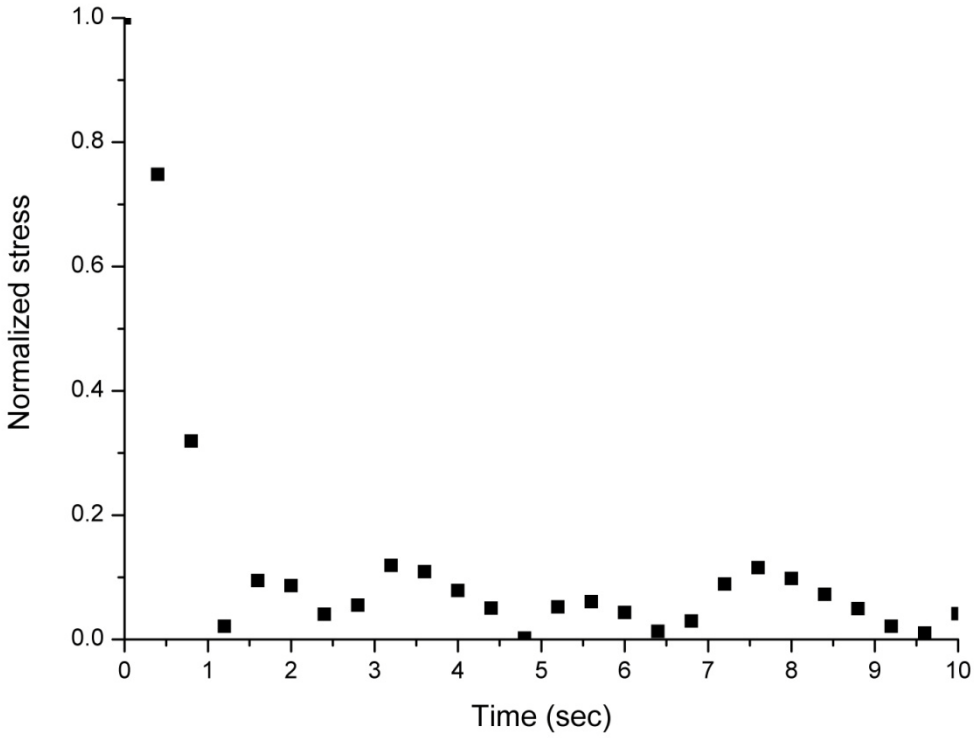

Figure 3.11 Experimental result of stress relaxation at 568°C (At+30°C).

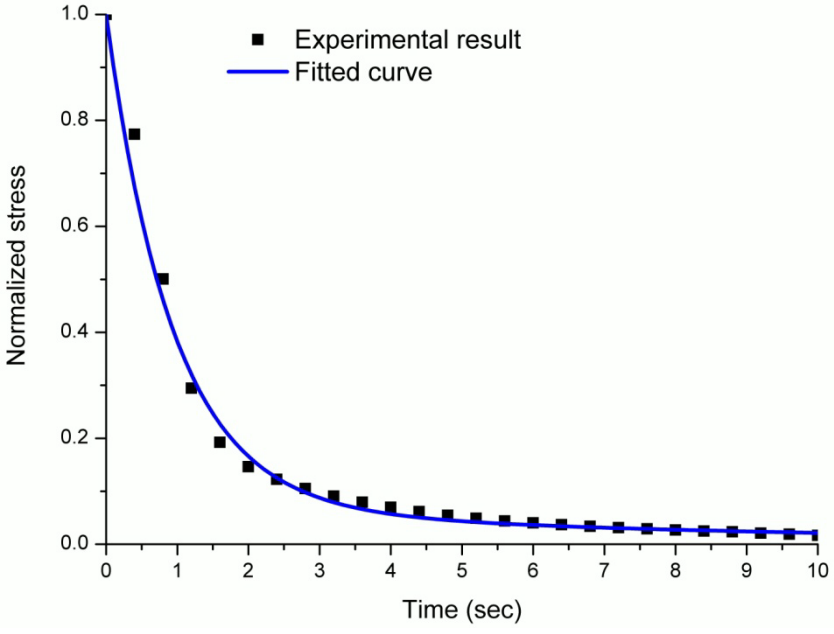

Figure 3.12 Experimental result of stress relaxation at 556°C (T_g+50°C) and the fitted curve.

Table 3.1 Structural relaxation parameters used in the FEA.

Reference temperature, T_{ref} (°C)	600
Fraction parameter, x	0.56
Weighing factor, w_g	Relaxation time, τ_p (sec)
0.448	0.0164
0.286	0.0059
0.266	0.0014

Table 3.2 Stress relaxation parameters used in the FEA.

Weighing factor, w_i	Relaxation time, τ_s (sec)
0.445	0.9360
0.484	0.9396
0.071	8.3305

CHAPTER 4 FEA AND VERIFICATION EXPERIMENT

Via material experiments, optical glass material properties for the FEA on the glass molding process in the heating and annealing stages were obtained. For the molding stage, because this study assumes that the optical glass behaves as Newtonian fluid, this assumption should be verified before being introduced into FEA. Therefore, in this chapter, a uniaxial compression experiment was first performed at the molding temperature and the experimental result was compared to the result obtained from FEA on the uniaxial compression with the Newtonian fluid assumption of the glass.

After these detailed optical glass material properties were all obtained, a FE model on the glass molding process was constructed. An optical glass lens molding experiment was performed to verify the feasibility of this FE model. Detailed results and discussions are presented in the rest of this chapter.

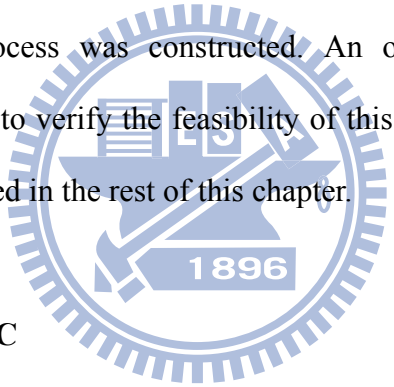

4.1 FEA Program - MARC

Marc (MSC. Software) is a commercial FEA program which is powerful to deal with nonlinear problems including geometric nonlinearities (metals bending), material nonlinearities (elastomers and metals that yield under structural or thermal loading) and boundary nonlinearities (contact problem). User subroutines and choices for Coulomb or shear friction make its usage more flexible.

Because the FEA on optical glass lens molding process includes self-defined material property (user subroutine) and glass to molds contact (contact problem with shear friction), MARC is an ideal choice for this research.

4.2 Verification on Newtonian Fluid Behavior at Molding Temperature

In the molding process, after pure thermal expansion of the glass and molds in the heating stage, the subsequent molding stage forms the basic profile of the lens. To accurately predict the lens profile, the mathematical model of the optical glass in the molding stage must represent the behavior of glass closely.

Section 2.3.2 had described that the optical glass behaves as a Newtonian fluid at the molding temperature when subjected to an applied load, and the mathematical model can be represented by eq. (2.10). To verify the accuracy of this model, a uniaxial compression experiment was performed at the molding temperature (568°C) and compared to the FEA result.

The compression test was performed in the same experimental apparatus, mentioned in section 3.3. Cylindrical specimen with 8mm in diameter and 8mm in height was used. Strain rate was held at 0.01/s, and the experiment was conducted without lubricant. Tooling steel was used for the molds.

Figure 4.1 shows the FE model for the uniaxial compression experiment. The glass specimen was modeled with 3200, four-node, axisymmetric, quadrilateral elements. Because the glass is much softer than the molds, both the upper and lower molds were set as rigid bodies in the simulation. Newtonian fluid model was introduced into FEA to describe the flow behavior of the glass specimen.

The interfacial friction between the glass and molds is described by:

$$\tau = mk_m \tag{4.1}$$

where τ is the shear stress of the interface, m is the shear factor ($0<m<1$), and k_m is the shear strength of the glass near the interface. This study uses a shear friction factor of 1.0, which assumes complete sticking between the glass preform and the molds.

Figure 4.2 shows the force-displacement relationship of the FEA and experimental

results. The FEA result is close to the result of compression test. This means the Newtonian fluid model is suitable to describe the flow behavior of the optical glass at the molding stage.

4.3 Optical Glass Lens Molding Experiment

An optical glass lens molding experiment was conducted on GMP-207HV (Toshiba Machine Co.), as shown in Figure 4.3, which is capable to set the molding temperature up to 1500°C, to apply pressing force ranging from 0.2 to 20kN and to provide vacuum or nitrogen environment. Embedded infrared lamps are used to heat the molds and the glass preform. Nitrogen gas is used to purge air from the chamber before the molding step to prevent oxidation of the mold and it is also used to control cooling rate of the mold assembly during the annealing stage. Figure 4.4 shows the schema of this apparatus.

An industrial lens design consisting of two aspherical surfaces was used in the molding experiment. Aspherical surfaces on both sides can be described by the following equation:

$$z(r) = \frac{r^2/R}{1+\sqrt{1-(1+K)r^2/R^2}} + A_4 r^4 + A_6 r^6 + A_8 r^8 + A_{10} r^{10} \qquad (4.2)$$

where R is the radius of curvature, K is the conic constant, and A_4, A_6, A_8, and A_{10} are the coefficients of the aspherical surfaces. Table 4.1 lists these coefficients.

The molds were made of tungsten carbide (Fujidie Co.) with Pt-Ir coating on the molding surfaces and finely ground to $\lambda/4$ (λ=632.8nm) of surface roughness to prevent surface features from imprinting onto the lens.

A glass preform with two spherical surfaces (shown in Figure 4.5) was used for the verification experiment. The thickness, radius of curvature, and diameter of the preform were designed using the optical design software, Zemax. Both the radius of curvature of

the preform surfaces were designed smaller than the radius of curvature of the corresponding lens surfaces to avoid air trapped between the mold and the glass preform during molding process. Surface roughness of the preform was set between 1~2 λ (λ=632.8nm).

The whole molding process can be divided into three stages: (1) Heating the glass preform and molds to the molding temperature, i.e. 568°C, (2) Molding the glass preform at 568°C (adiabatically) with a compressive force of 1kN and maintaining the force for 120 sec, (3) Step cooling control with an initial rate of 0.5°C/sec to 420°C. A subsequent cooling was controlled by the nitrogen flow rate. The formed lens was removed upon reaching the mold releasing temperature, 200°C. Figure 4.6 shows the schematic of the processing history.

4.4 FEA Model and Boundary Conditions

Figure 4.7 to Figure 4.9 show the boundary conditions of the FE models and the inputted glass material models of each stage. The FE models use four-node, axisymmetric, thermo-mechanically coupled, quadrilateral elements. The glass preform was modeled with 9462 elements and the upper and lower molds were modeled with 5160 elements. Simulation settings were the same as those in the molding experiments.

Table 4.2 summarizes the mechanical and thermal properties of the glass and molds used in this simulation. The molds were treated as elastic bodies (with a thermal expansion property) throughout the simulation. The interfacial friction between the glass and molds is assumed as complete sticking (i.e. m=1) between the glass preform and the molds.

4.5 Optical Glass Lens Molding Experimental and FEA Results

Because the lens shape is primarily determined in the molding stage, the material model introduced is critically related to shape prediction accuracy. The Newtonian flow behavior in the molding stage can be verified by observing the time-displacement relationship between the experimental and simulated results. Figure 4.10 shows a good agreement between these results, indicating that the Newtonian flow indeed accurately describes the deformed shape before annealing.

Because the stresses generated in the molding stage are relaxed instantly owing to high molding temperature (568°C) and low viscosity ($10^{8.35}$ Pa·s), the residual stresses in the lens product are all induced owing to the thermal strain in the annealing stage. The FEA predicted lens shape and residual stress were obtained by incorporating the structural relaxation and stress relaxation properties in the annealing stage. Figure 4.11 shows the simulated final lens shape together with predicted residual stresses.

Residual stress results in stress birefringence. According to ISO 10110-2 [37], the birefringence produces a difference in index of refraction in the glass for light polarized parallel or perpendicular to the residual stress. This can affect the wavefront quality or optical path difference of the light transmitted through the optical element. The residual stress induced birefringence is specified in terms of OPD of retardation. This is given by the equation:

$$OPD = a \cdot s \cdot c \tag{4.3}$$

where OPD is the optical path difference in nm, a is the sample thickness in cm, s is the residual stress in units of N/mm^2 and c is the difference in the photoelastic constants in units of $10^{-7} mm^2/N$. A retardation of more than 10nm/cm sample thickness generally corresponds to “coarse” annealed glass while a retardation of less than 10nm/cm sample thickness refers to “fine” annealed glass, typical for precision optical elements. For L-BAL42, c is not specified by the manufacturer, and we assume c is 0.2 by

referring to glass with similar compositions. According to the simulated results, the max OPD was about 1.60nm/cm sample thickness in the outer lens and the OPD was about 1.16nm/cm sample thickness in the center, indicating that the cooling process was a fine annealing process. Because the birefringence measurement on the molded lens to measure the residual stress in the lens is difficult to achieve with current apparatus, future studies can keep searching for a suitable apparatus to perform this measurement for experimental verification.

In the FEA prediction, a larger residual stress appears close to the upper surface of the lens. This is because the upper mold cools slightly faster than the lower mold, inducing a larger temperature difference close to the upper surface and resulting in a larger residual stress in this area.

Predicted thickness in the center of the lens is 4.843mm, and the final lens diameter is 21.551mm. Figure 4.12 shows the lens formed in the molding experiment. The central thickness was 4.838mm (measured using Mitutoyo IDC digimatic indicator (543-251) with 0.003mm accuracy). The average diameter was 21.665mm which was calculated by averaging the measured values in four equally divided directions (values were measured using Mitutoyo dial caliper (505-666) with 0.01mm accuracy). Deviations between the verification experimental results and the simulated results are 0.103% in thickness and -0.526% in diameter. Table 4.3 summarizes these shape differences. These results indicate that incorporating structural relaxation allows an accurate prediction of the thickness and diameter.

Figure 4.13 compares the experimental and simulated surface curve results and Figure 4.14 shows the deviations between the simulated and experimental surface curves. Table 4.4 shows the root mean square and absolute values of deviations. Deviations on the upper surface (RMS: 0.559μm and absolute max: 1.972μm) are slightly larger than deviations on the lower surface (RMS: 0.290μm and absolute max:

1.167μm). This implies that the real temperature distributions on each lens surface may not be uniform, unlike those in the FEA. The temperature distributions were inputted uniformly on each lens surface in the FEA and the inputted temperature histories were measured by single thermo-couples embedded in each mold. Figure 4.15 shows the FEA inputted temperature distribution and temperature history. With the uniform temperature input, the variations of the surface curves predicted by FEA before and after annealed are shown in Figure 4.16. The directions of variation reductions for each surface curves during and after annealing are shown in Figure 4.17. The directions of variation reductions change suddenly at a point about 5mm from the center in the radius direction for the upper surface and about 5.3mm for the lower surface. By comparing both the experimental and simulated surface curves after annealing to the designed ones, as shown in Figure 4.18 and Figure 4.19, deviations are found to be increased after the above mentioned changing points of the reduction directions. For the upper surface, this may indicate that the cooling rate is slower near the outer lens than that in the lens center, thus results in smaller values of reduction than those predicted by the FEA with uniform temperature distribution. For the lower surface, the experimental and simulated results are very close. Small deviations near the outer lens may indicate that the cooling rate is faster than that in the lens center, thus results larger values of reduction than those predicted by the FEA with uniform temperature distribution. Future study is expected to conduct multi-point measurements of the temperature distribution on the lens and molds surfaces to obtain the real temperature distributions. Also, a more complex thermal model that considers heat transfer between the molds, lens, and the atmosphere inside the furnace can be constructed in the future by referring to related studies and conducting multi-points temperature measurements to enhance the FEA prediction capability on the optical glass molding process.

Figure 4.20 and Figure 4.21 show the deviations of the experimental and simulated surface curves from the designed ones after annealing. FEA results with and without stress and structural relaxation properties are shown in these two figures. Table 4.5 shows the RMS values of the surface curve deviations between experimental and FEA results. These results show that the simulated results with stress and structural relaxation properties are more close to the experimental ones than the simulated results without these two properties. Moreover, Figure 4.22(a) and Figure 4.22(b) show that the residual stresses in the lens after annealing can be predicted only by incorporating stress and structural relaxation properties. The simulated surface curves and the residual stresses all indicate that incorporating the stress and structural relaxation into FEA in the annealing stage enhances the prediction accuracy and is necessary for the FEA on the optical glass molding process.

Despite the small discrepancy on surface curve prediction, the lens shape was accurately predicted in this study. Thus it can be concluded that the FE model of this study is useful for providing industrial design references.

4.6 Further Discussions on the Forming Parameters

4.6.1 Molding force and molding time

Three different molding forces and three different molding times were further tested in the FEA. Figure 4.23 to Figure 4.30 show the simulated final lens shapes together with predicted residual stresses. Table 4.6 shows the predicted central thicknesses of the formed lens, and Table 4.7 shows the diameter of the formed lens. It can be seen that under the same molding force, longer molding time causes thinner central thickness and larger diameter of the formed lens. It is also observed that under the same molding time, larger molding force causes thinner central thickness and larger diameter of the formed lens. Therefore, increasing the molding force and

reducing the molding time can effectively reduce the whole processing time.

The simulated final lens shapes, which were formed under various molding forces and molding times, as shown in Figure 4.23 to Figure 4.30, were obtained by using the same annealing conditions. The relationships between different lens profiles and the induced residual stresses were investigated. It is found that the lens with thicker central thickness possesses larger residual stresses in the lens center. This is because that the lens with thicker central thickness possesses larger temperature variation in the lens center, thus results in larger residual stresses after annealing. Therefore, different annealing conditions, such as different cooling rates, should be adopted for different lens shapes to minimize the residual stresses in the lens product.

4.6.2 Cooling rate

Two initial cooling rates, 0.3°C/sec and 0.5°C /sec, were also introduced into FEA (the same cooling rates were inputted in both the upper and the lower molds) to discuss their effects on the formed lens. Table 4.8 shows the simulated diameter and central thickness of the lens. The predicted diameter (21.552mm) and central thickness (4.843mm) of the lens with initial 0.3°C/sec cooling rate are smaller than the diameter (21.558mm) and the central thickness (4.844mm) of the lens with initial 0.5°C/sec cooling rate. These results indicate that the optical glass lens indeed formed into a denser structure with a slower cooling rate owing to the structural relaxation property.

Figure 4.31 shows the predicted residual stresses with different cooling rate. The predicted residual stresses with the initial 0.5°C/sec cooling rate are higher than the residual stresses with the initial 0.3°C/sec cooling rate. These predicted residual stresses show that in the annealing stage, faster cooling rate induces higher residual stresses owing to the structural and stress relaxation properties of the glass. Therefore,

in the annealing stage, the cooling rate should be kept as slow as possible to minimize the residual stresses in the lens product.

4.7 Summary

The Newtonian fluid behavior of the glass in the molding stage was verified by comparing uniaxial compression experimental result to that of the FEA one. With this verified material property, a complete material model for the optical glass molding process had been constructed by incorporating other experimental obtained material properties, i.e. coefficients of thermal expansion, structural relaxation property and stress relaxation property, obtained from dilatometric measurement, DSC measurement and stress relaxation respectively. After performing an optical glass lens molding experiment that followed the same protocol used in industry, the comparison of the molded lens shape as well as the surface curve deviation verified the accuracy of this FE model. Forming parameters such as molding force, molding time and cooling rate were also discussed by FEA and can be verified experimentally in the future.

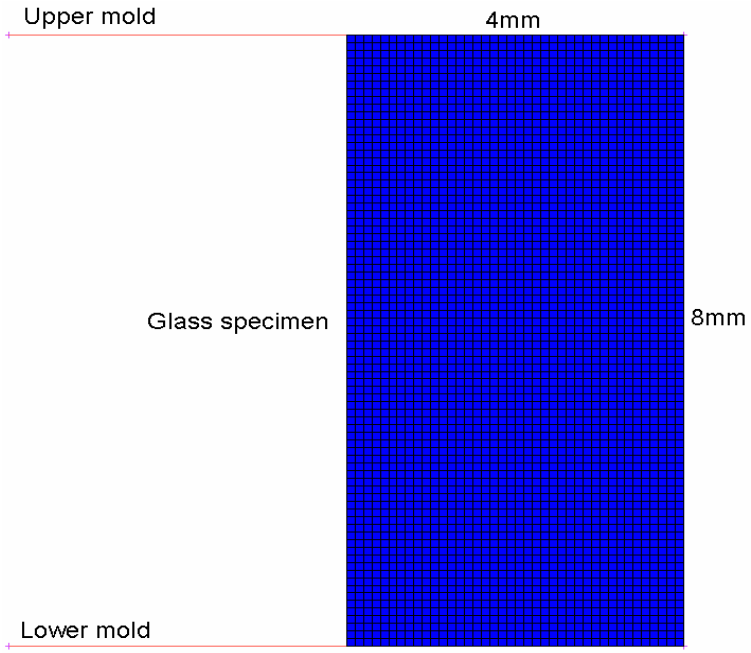

Figure 4.1 2D axisymmetric FEA model of the compression test.

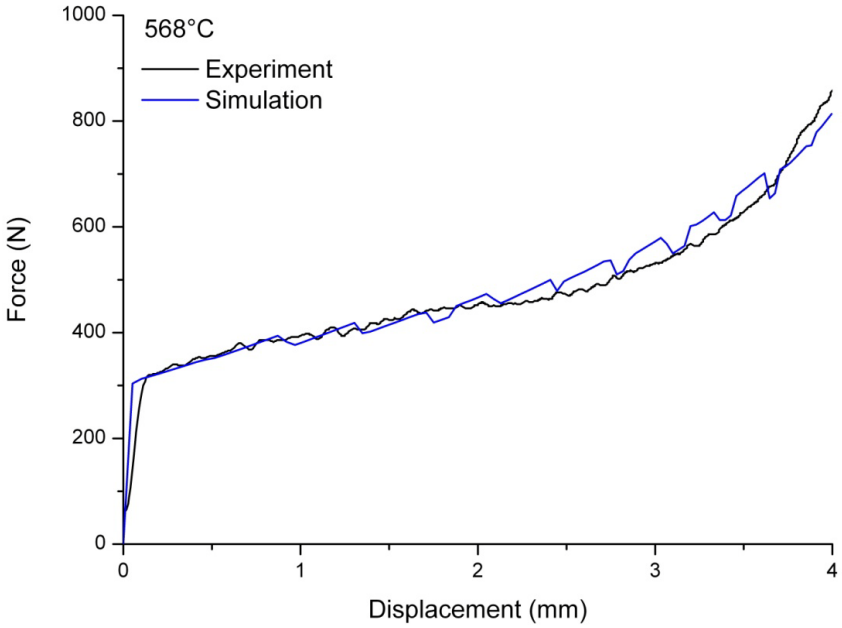

Figure 4.2 Force-displacement relationship of the compression test at molding temperature (568°C).

Figure 4.3 Optical glass lens molding apparatus GMP-207HV (Toshiba Machine Co.)

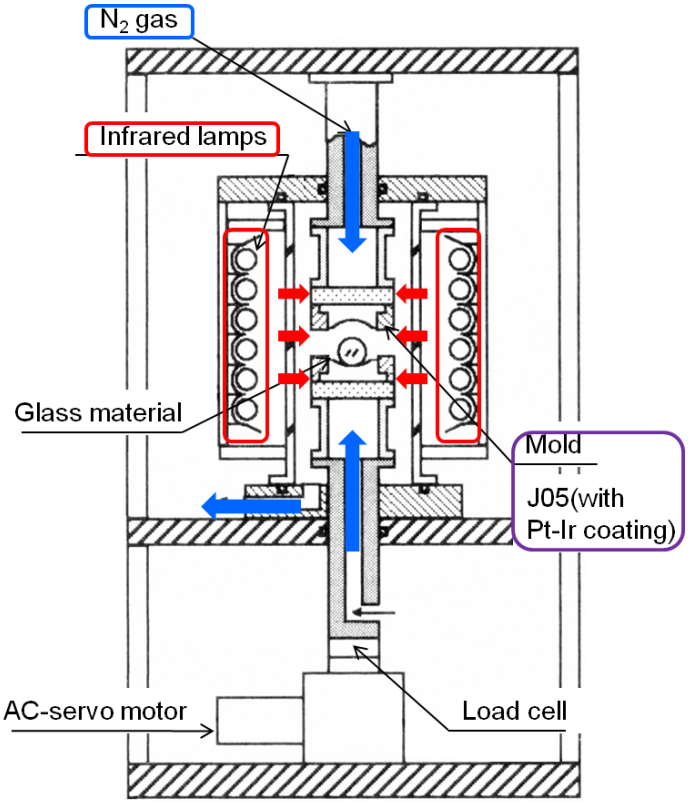

Figure 4.4 Schema of the optical glass lens molding apparatus GMP-207HV (Toshiba Machine Co.)

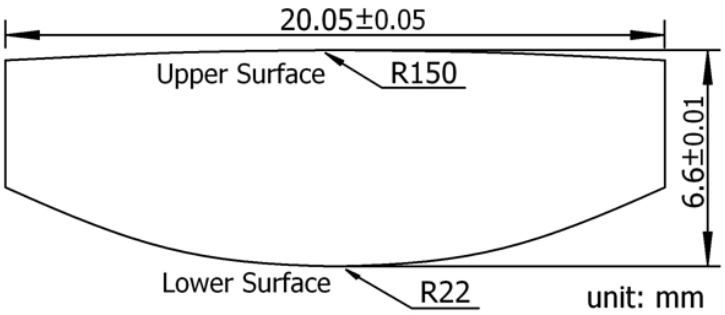

Figure 4.5 Schematic of the glass lens preform.

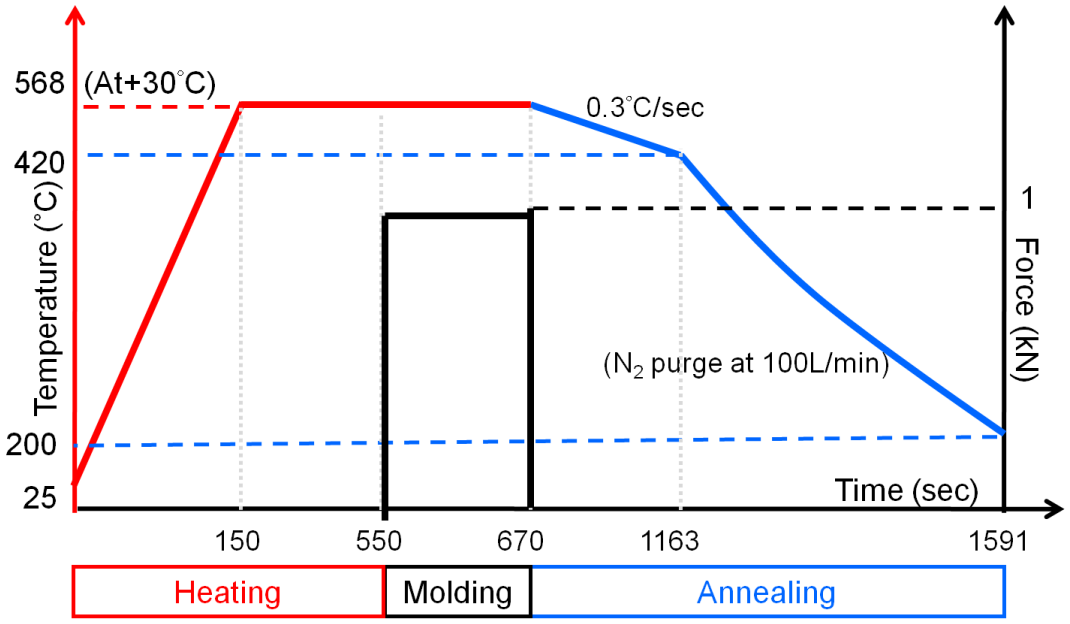

Figure 4.6 Temperature and applied force history of the glass molding process.

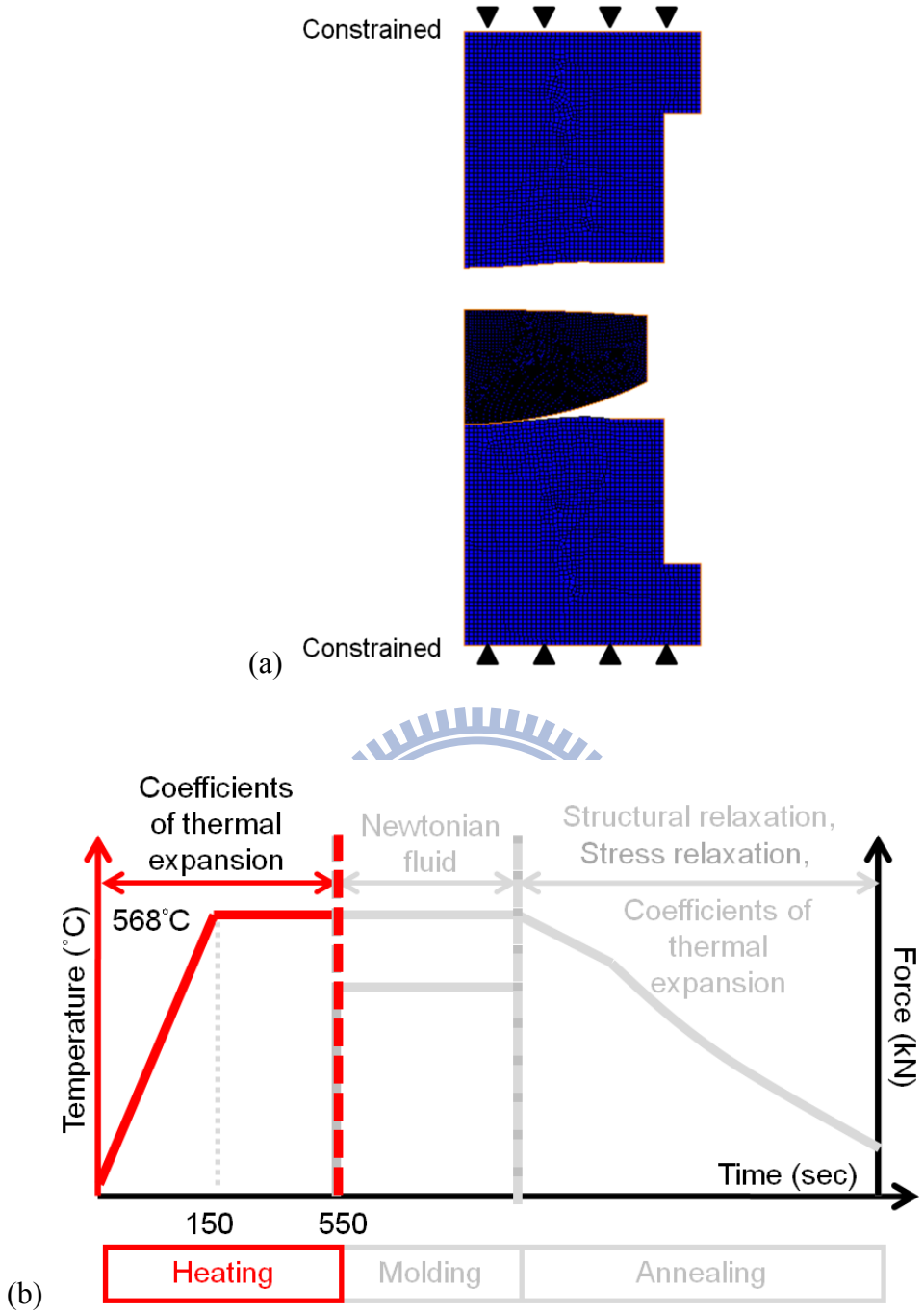

Figure 4.7 2D axisymmetric FEA model of the glass molding process (heating stage).

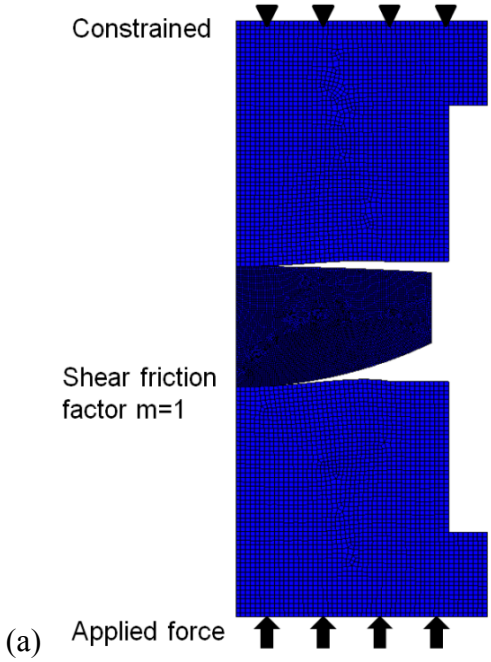

(a)

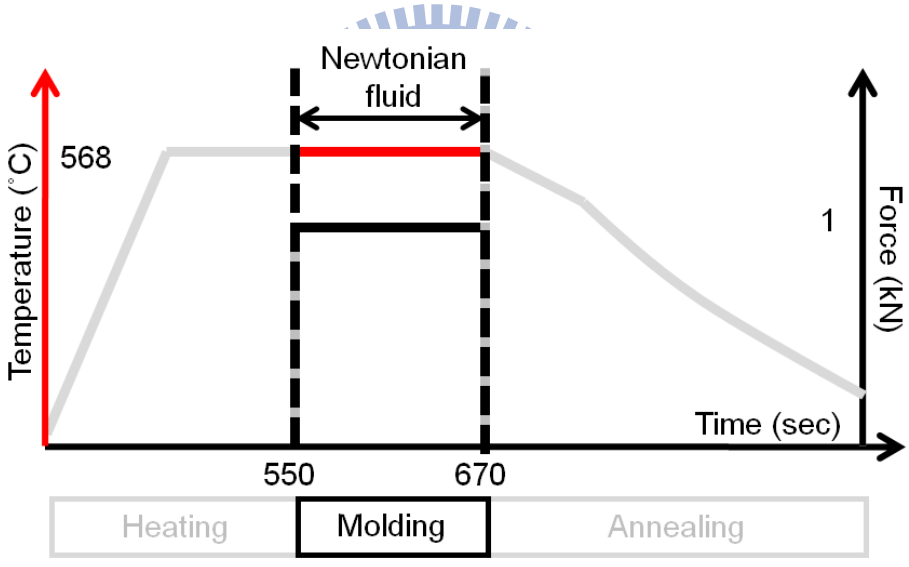

(b)

Figure 4.8 2D axisymmetric FEA model of the glass molding process (molding stage)

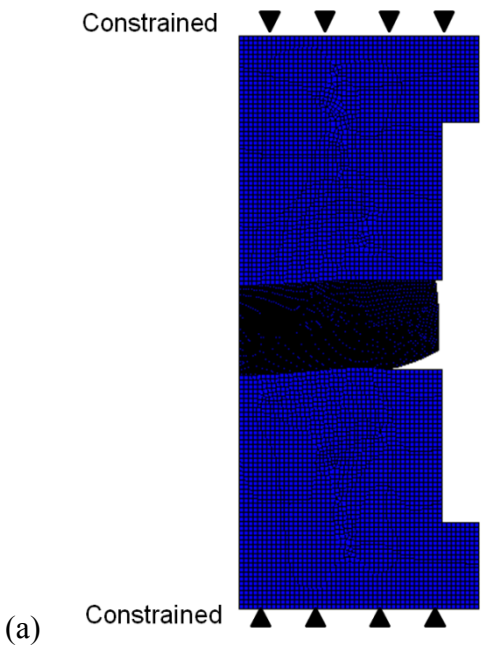

(a)

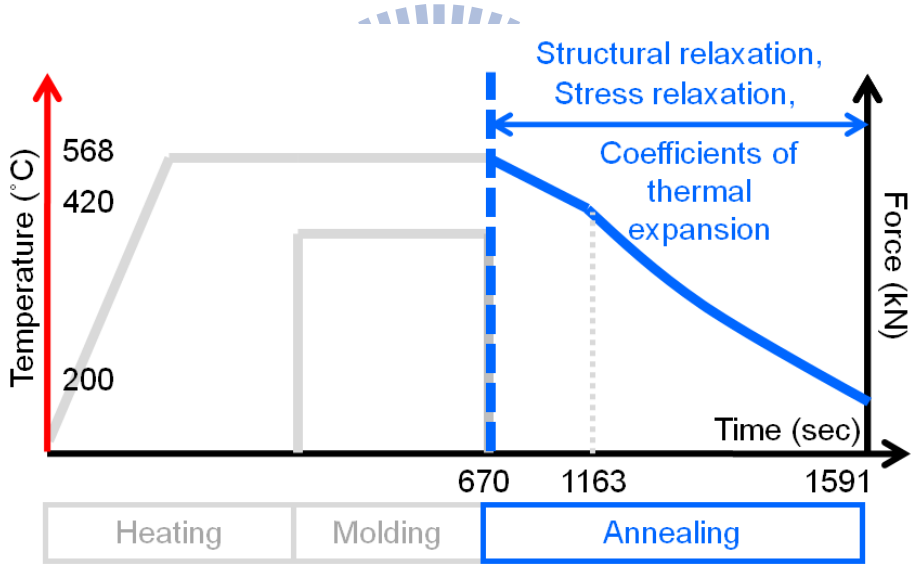

(b)

Figure 4.9 2D axisymmetric FEA model of the glass molding process (annealing stage).

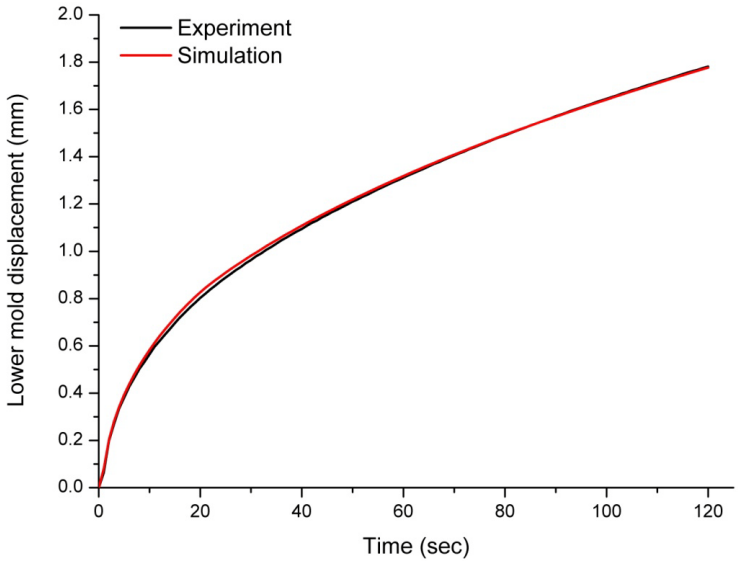

Figure 4.10 Molding time-displacement relationship in the molding stage.

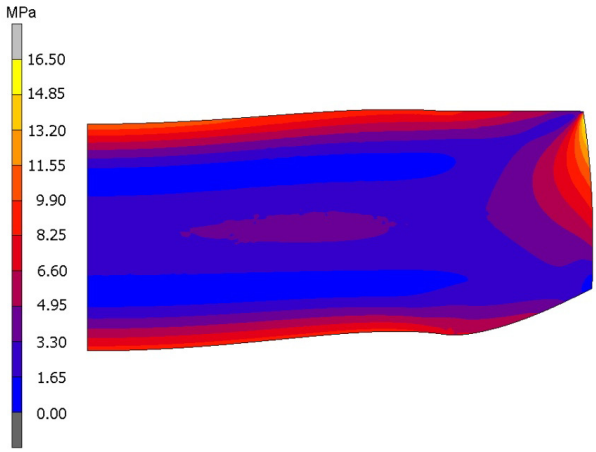

Figure 4.11 Simulated lens shape and predicted residual stress (equivalent von Mises stress).

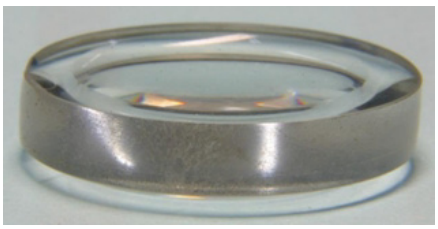

Figure 4.12 Verification experiment molded lens.

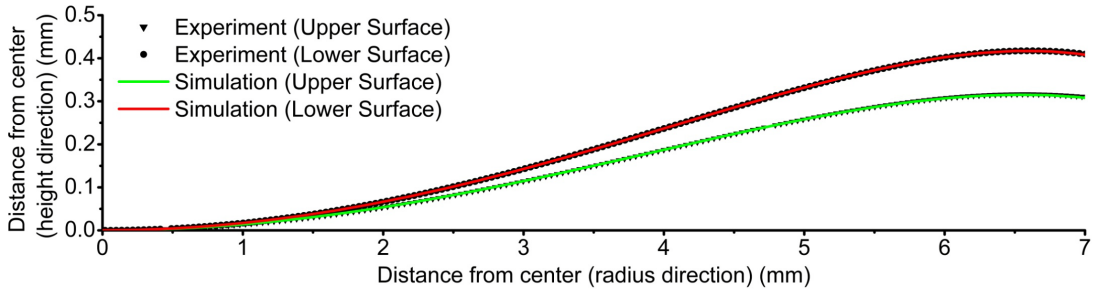

Figure 4.13 Surface curves of the experimental and simulated results.

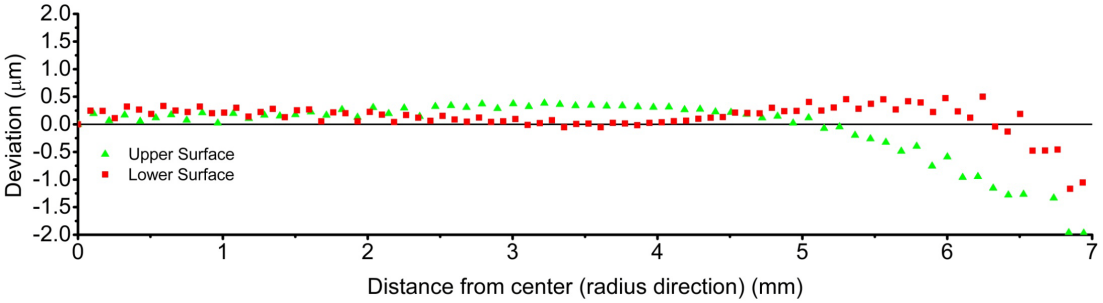

Figure 4.14 Deviations of the simulated surface curve from the experimental surface curve.

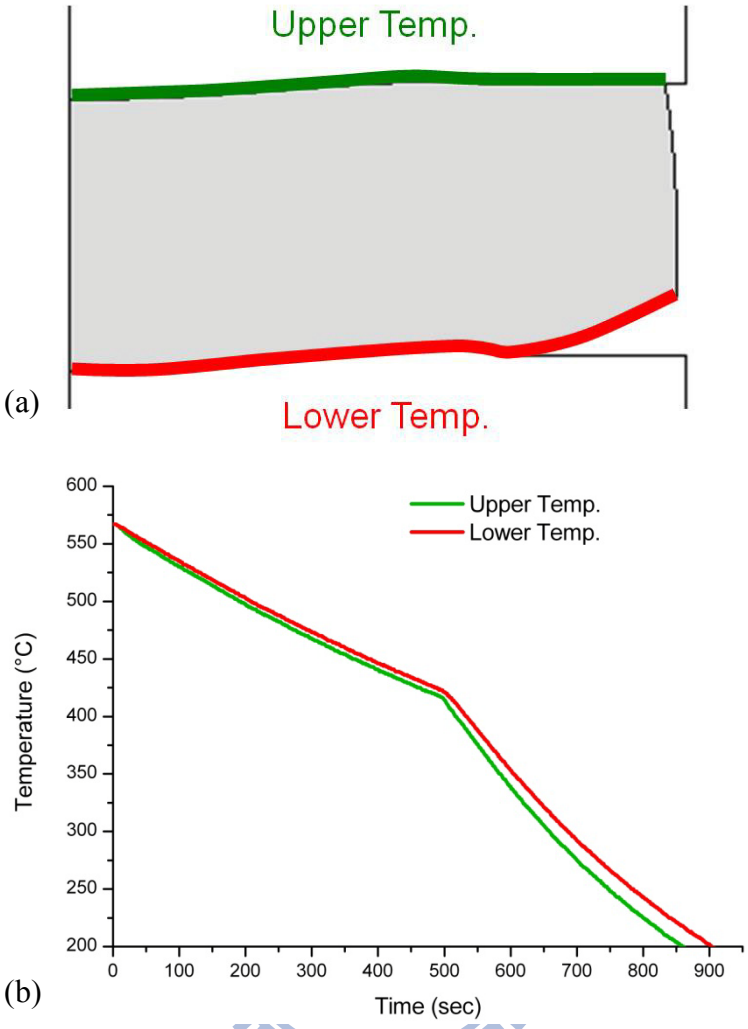

Figure 4.15 FEA inputted temperature distribution and temperature history (a) schematic of uniform temperature distribution (b) inputted temperature history.

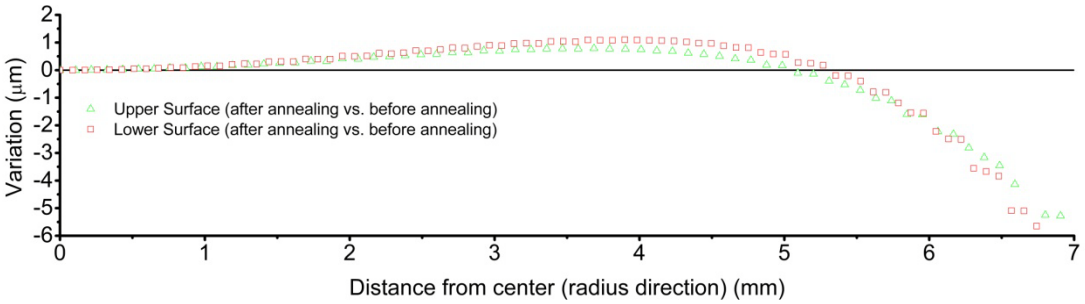

Figure 4.16 Variations of surface curves before and after annealing.

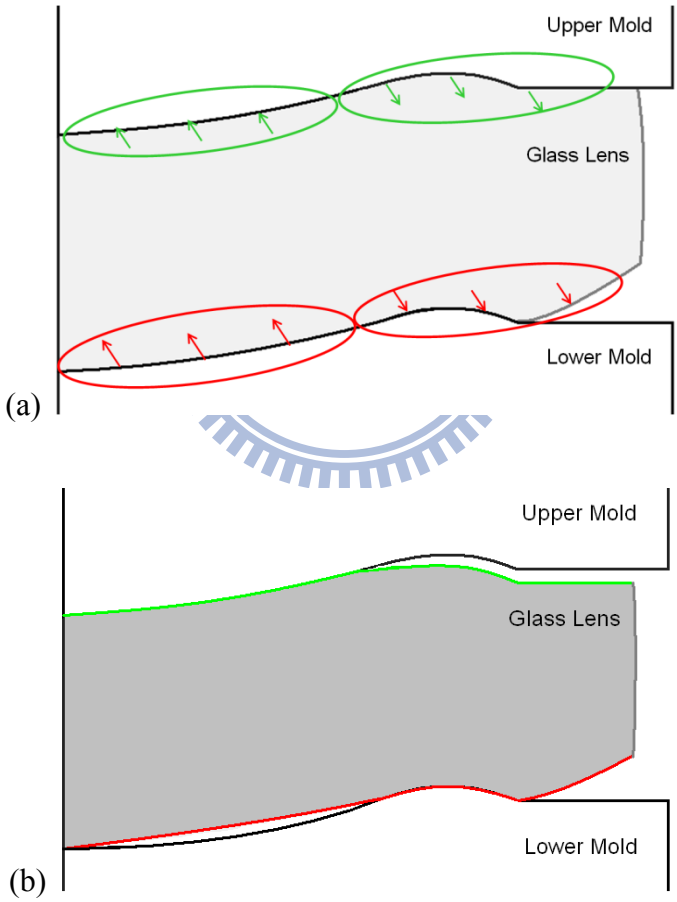

Figure 4.17 Directions of variation reduction of the surface curves (a) during annealing (b) after annealing (green area indicates the upper surface and red area indicates the lower surface)

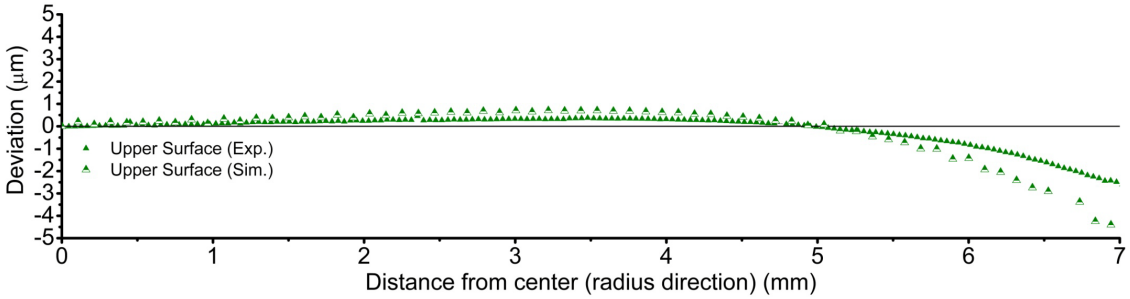

Figure 4.18 Deviations of the experimental and simulated surface curves from the designed curve after annealing (upper surface)

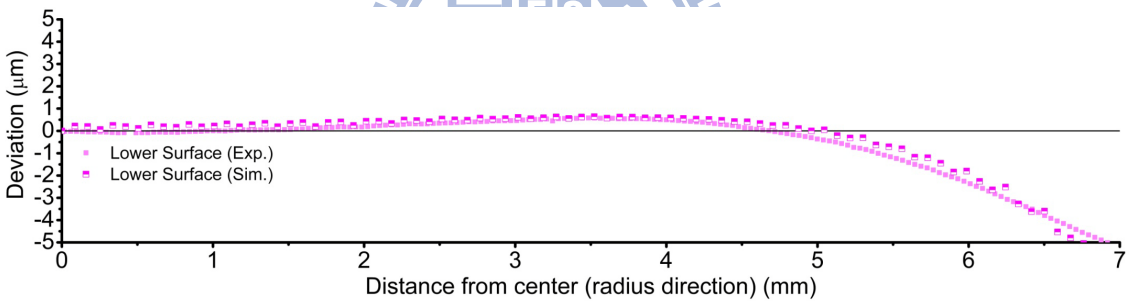

Figure 4.19 Deviations of the experimental and simulated surface curves from the designed curve after annealing (lower surface)

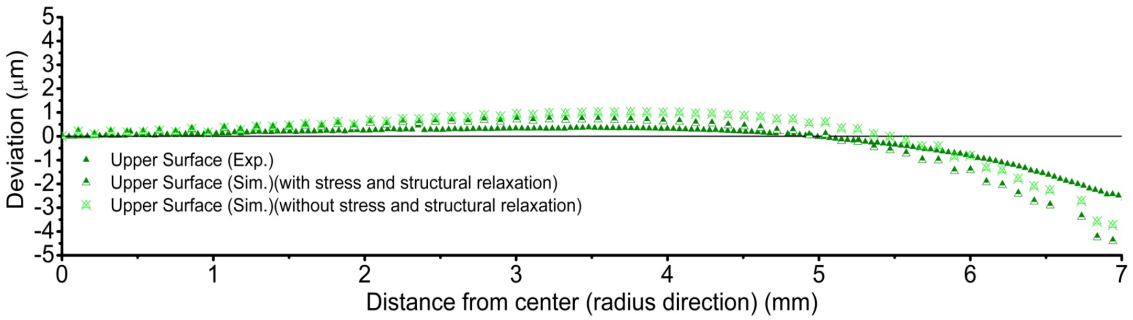

Figure 4.20 Deviations of the experimental and simulated surface curves from the designed curve after annealing (upper surface).

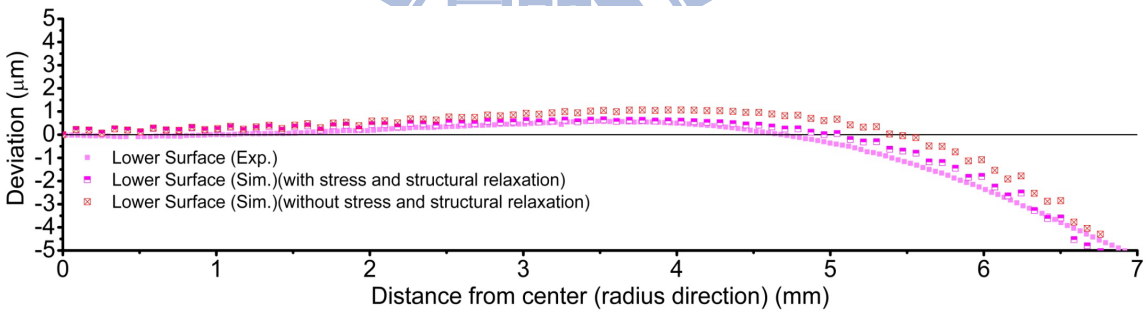

Figure 4.21 Deviations of the experimental and simulated surface curves from the designed curve after annealing (lower surface)

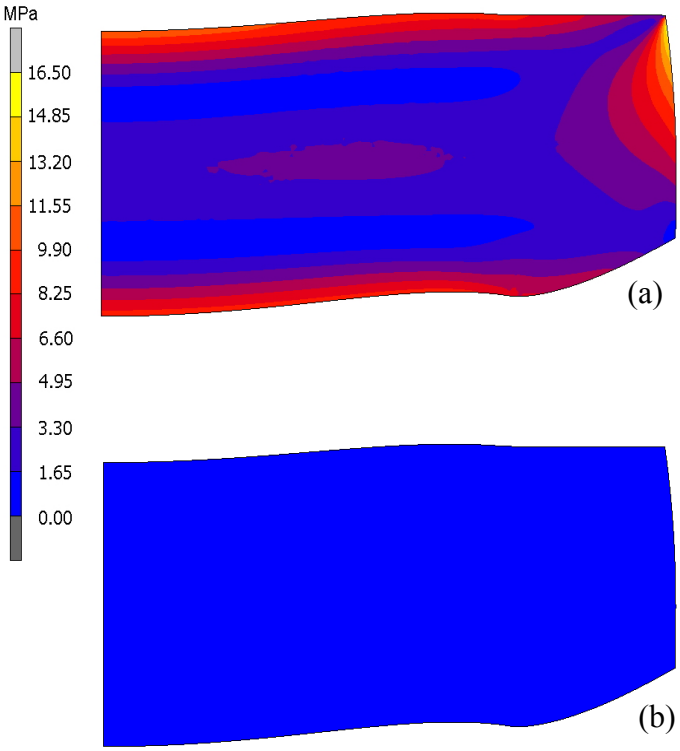

Figure 4.22 Simulated lens shape and predicted residual stress (a) with stress and structural relaxation (b) without stress and structural relaxation (equivalent von Mises stress).

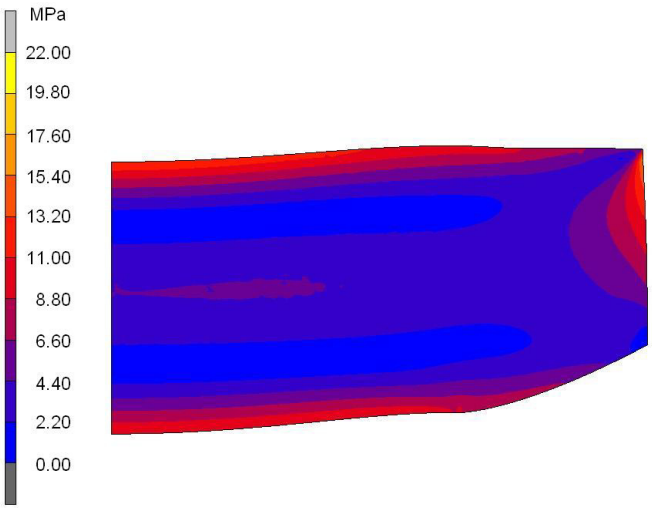

Figure 4.23 Simulated lens shape and predicted residual stress (molding force: 1kN, molding time: 60sec) (equivalent von Mises stress).

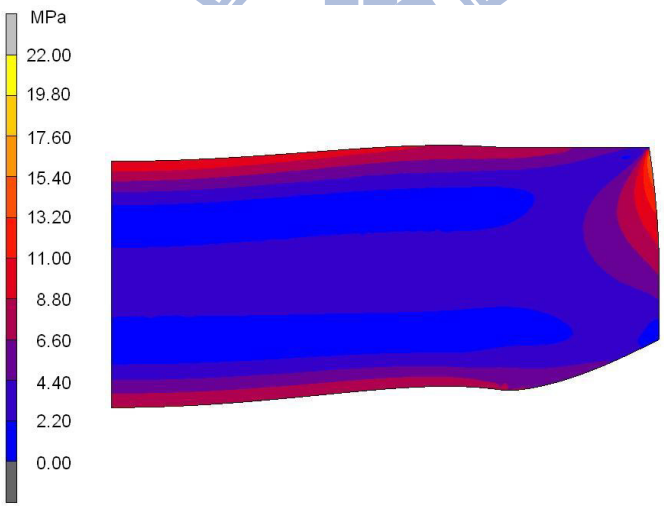

Figure 4.24 Simulated lens shape and predicted residual stress (molding force: 1kN, molding time: 120sec) (equivalent von Mises stress).

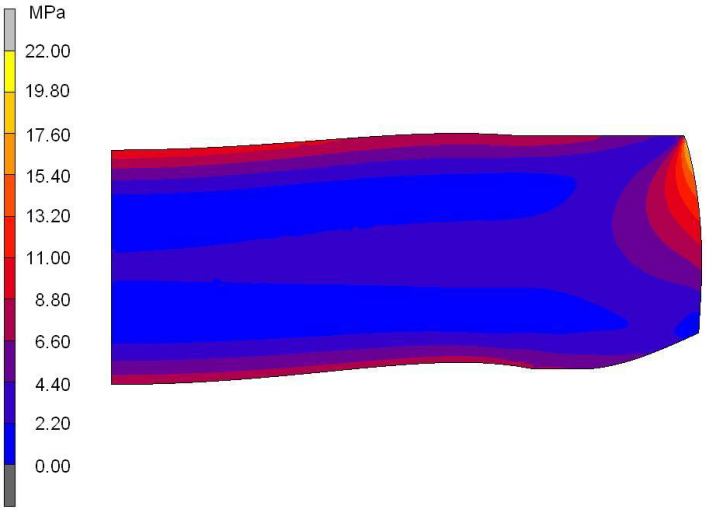

Figure 4.25 Simulated lens shape and predicted residual stress (molding force: 1kN, molding time: 200sec) (equivalent von Mises stress).

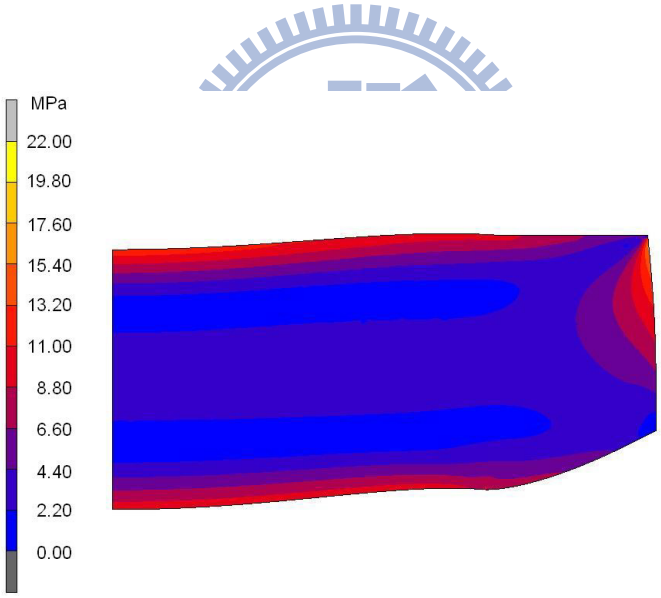

Figure 4.26 Simulated lens shape and predicted residual stress (molding force: 1.5kN, molding time: 60sec) (equivalent von Mises stress).

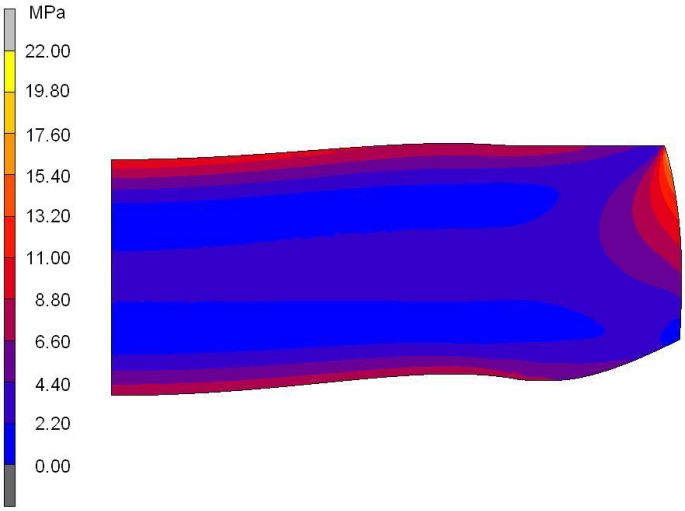

Figure 4.27 Simulated lens shape and predicted residual stress (molding force: 1.5kN, molding time: 120sec) (equivalent von Mises stress).

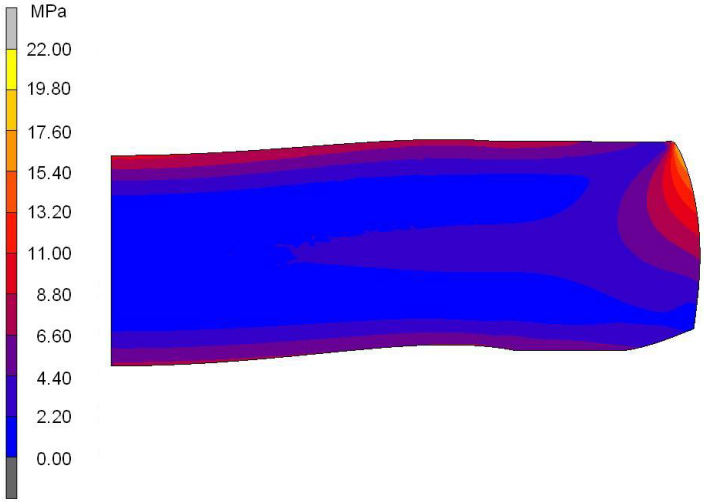

Figure 4.28 Simulated lens shape and predicted residual stress (molding force: 1.5kN, molding time: 200sec) (equivalent von Mises stress).

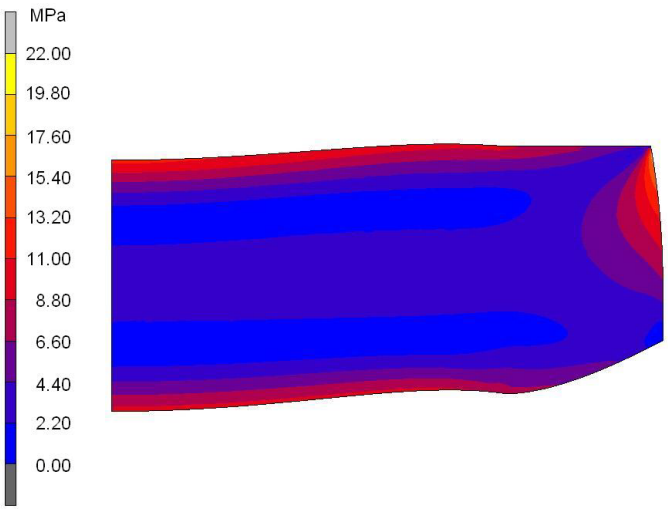

Figure 4.29 Simulated lens shape and predicted residual stress (molding force: 2kN, molding time: 60sec) (equivalent von Mises stress).

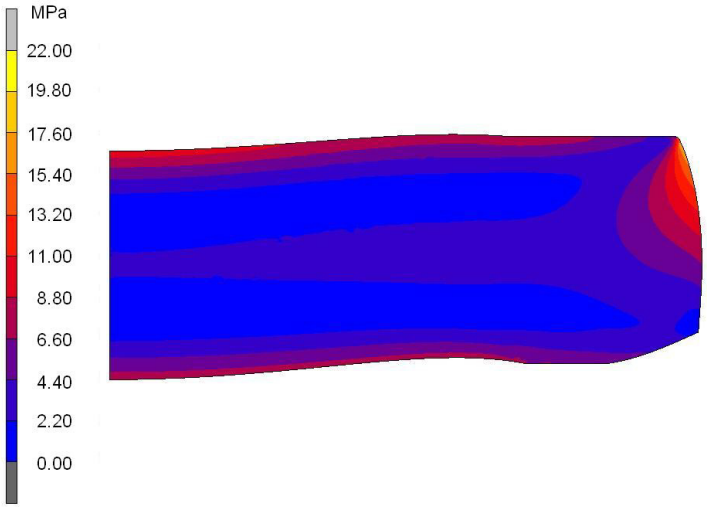

Figure 4.30 Simulated lens shape and predicted residual stress (molding force: 2kN, molding time: 120sec) (equivalent von Mises stress).

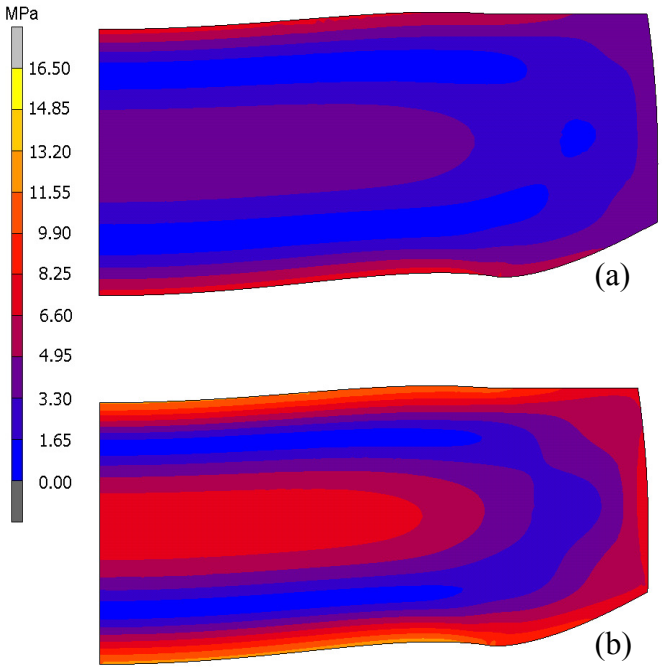

Figure 4.31 Simulated lens shape and predicted residual stress (a) cooling rate 0.3°C/sec (b) cooling rate 0.5°C/sec (equivalent von Mises stress).

Table 4.1 Coefficients of aspherical surfaces.

	Lower Surface	Upper Surface
Radius of curvature (R)	29.36279	36.20536
Conic constant (K)	-2.356642	5
Fourth order of coefficient (A_4)	-1.2073499×10^{-4}	-1.3695827×10^{-4}
Sixth order coefficient (A_6)	-9.0520309×10^{-7}	-9.0581284×10^{-7}
Eighth order coefficient (A_8)	1.2735685×10^{-10}	5.2370159×10^{-9}
Tenth order coefficient (A_{10})	-2.8993811×10^{-11}	-5.5728842×10^{-12}

Table 4.2 Mechanical and thermal properties of glass [35] and molds [36].

	Glass (L-BAL42)	Mold (J05)
Elastic modulus (GPa)	89.1	650
Poisson's ratio	0.247	0.20
Density (g/cm^3)	3.05	14.65
Thermal conductivity (W/m°C)	1.03	63
Specific heat (J/kg°C)	622.9	314
Linear coefficient of thermal expansion (1/°C)	Liquid state: 9.17×10^{-5} Glassy state: 9.12×10^{-6}	4.8×10^{-6}

Table 4.3 Lens shape differences between experimental and experimental results

	Diameter (mm)	Central thickness (mm)
Experiment	21.665	4.843
FEA result	21.551	4.838
Error	-0.526%	0.103%

Table 4.4 Surface curve deviations between experimental and FEA results.

	Absolute max. (mm)	RMS (mm)
Upper surface	1.972	0.559
Lower surface	1.167	0.290

Table 4.5 RMS values of the surface curve deviations between experimental and FEA results (with and without stress and structural relaxation).

	RMS (mm) (Upper surface)	RMS (mm) (Lower surface)
With stress and structural relaxation	0.559	0.290
Without stress and structural relaxation	0.588	0.632

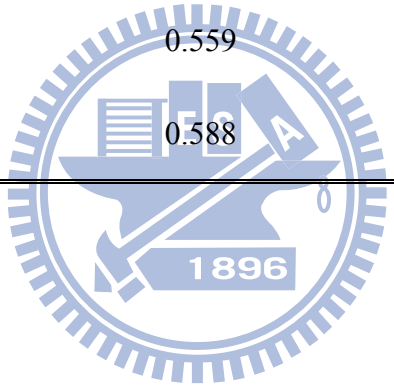

Table 4.6 Central thickness of the formed lens under various molding forces and molding times.

		Molding time (sec)		
		60	120	200
Molding force (kN)	1	5.297	4.843	4.427
	1.5	5.074	4.556	4.122
	2	4.891	4.345	--

Table 4.7 Diameter of the formed lens under various molding forces and molding times.

		Molding time (sec)		
		60	120	200
Molding force (kN)	1	20.909	21.665	22.322
	1.5	21.205	22.062	23.063
	2	21.480	22.525	--

Table 4.8 FEA results with different cooling rates (diameter and central thickness of the formed lens).

		Diameter (mm)	Central thickness (mm)
Cooling rates (°C/sec)	0.3	21.552	4.843
	0.5	21.558	4.844

CHAPTER 5 CONCLUSIONS AND FUTURE WORKS

Throughout this study, the following topics have been investigated:

(1) Thermal expansion experiment was performed to obtain detailed thermal expansion coefficients of the optical glass.

(2) DSC measurement on the variation of heat capacity was performed and the measured values were normalized and the fitted with equations to obtain the structural relaxation property of the optical glass.

(3) Uniaxial stress relaxation experiment on the optical glass was performed and the experimental result was converted by a relationship of shear and uniaxial stresses to obtain the shear stress relaxation properties for FEA input.

(4) Uniaxial compression experiment was performed at the molding temperature for verifying the assumption of adopting Newtonian fluid behavior for the glass in the molding stage.

(5) An optical lens molding experiment was performed and compared to FEA on the glass molding process to verify the feasibility of the FE model with these detailed optical glass material properties.

(6) The effect of forming parameters such as molding force, molding time and cooling rate were analyzed by FEA.

5.1 Conclusions

This study presents a precise material model for glass lens shape prediction that incorporates actual thermal expansion coefficients, structural relaxation properties, and stress relaxation properties obtained from material experiments. Through the above mentioned investigations, a comprehensive FEA model incorporating this material

model for lens shape prediction was verified by a molding experiment. The following summary concludes this study:

(1) Because the actual coefficients of thermal expansion in the glassy and liquid states determine the expanded shape at the beginning of the molding process, they are crucial for FEA in predicting the final lens shape. The two temperature-dependent coefficients of thermal expansion should be obtained from the glass manufacturer or from actual expansion experiments.

(2) Uniaxial compression test of glass L-BAL42 was performed at the molding temperature (568°C, 30°C above At), and the feasibility of the Newtonian fluid for glass material in the molding stage was verified by comparing the simulation results to the experimental data.

(3) DSC measurements on glass L-BAL42 were performed in this research and the obtained structural relaxation property was inputted into the FEA. For further investigation on the FEA applications of the glass molding process with different glasses, it is recommended to perform DSC measurement on the adopted glasses to obtain their structural relaxation properties.

(4) This research also conducted uniaxial compressive stress relaxation experiment on the glass and converted the result into shear relaxation properties by using a relationship between the uniaxial and shear stress relaxation time. The obtained shear stress relaxation property was then introduced into FEA.

(5) The FEA result reveals that incorporating the experimentally obtained structural relaxation and stress relaxation properties can accurately predict the formed lens

shape. Prediction on the residual stress inside the lens was also demonstrated with the aid of these two properties, and can be verified by refractive index measurements in the future.

(6) The effect of forming parameters such as molding force, molding time and cooling rates were analyzed by FEA in this study. Results show that increasing molding force and reducing molding time can effectively reduce the whole processing time. Also, to minimize the residual stresses in the formed lens, different annealing conditions should be adopted for different lens shapes and cooling rate should be kept as slow as possible.

5.2 Future Works

As concluded above, a comprehensive FEA on the glass molding process was done in this work. However, some topics can still be investigated in the future:

(1) For simplicity, this study does not consider the heat transfer between the glass, molds, and atmosphere within the furnace. Future study can firstly conduct multi-point measurements of the temperature distribution on the mold and the lens surfaces to obtain the real temperature distributions. By utilizing the measured information and referring to related studies, a more accurate thermal model can be constructed to consider heat transfer between the molds, lens, and the atmosphere inside the furnace to enhance the FEA prediction capability of the glass molding process.

(2) Pre-compensation of the molds by using an optimization system can be investigated in the future. Wu [38] made attempts to construct an optimization

system for the pre-compensation on the mold design, but the material properties of the glass was not completed at that time. Since the complete material model of the glass molding process is established now, it is suitable to incorporate the optimization system into FEA to construct an automatic pre-compensation system of the molds and therefore provide a reference for the industry.

(3) An optimization system which is flexible to observe the influences of forming parameters such as molding force, holding time, cooling rate, etc. can be constructed further. Because different glass material corresponds to different set of optimal forming parameters, finding a better set of parameters is always a difficult task for engineers. Based on this work, the development of an optimization system to acquire the optimal forming parameters automatically will be very useful for the glass molding industry.

(4) Forming microstructures on the glass lens surface such as micro lens array or fiber array by glass molding is an interesting issue. Because the scale of microstructures is relatively smaller than the glass substrate, forming parameters are more critical than ordinary lens forming. To achieve a qualitative product is also much difficult. Future studies can utilize this comprehensive FEA into this microstructure forming process and help solving some critical obstacles.

REFERENCES

[1] ITRC, 2007, *Precision Manufacturing & Inspection of Optical Components*, Instrument Technology Research Center.

[2] Jain, A., 2006, *Experimental Study and Numerical Analysis of Compression Molding Process for Manufacturing Precision Aspherical Glass Lenses.* Ph.D thesis, Industrial and Systems Engineering, The Ohio State University.

[3] http://commons.wikimedia.org/wiki/File:Lens_spherical_aberration.png

[4] http://www.dcfever.com/learn/viewglossary.php?glossary_id=45

[5] Amgle, M. A., Blair, G. E., Maier, C. C., 1974, Method for molding glass lenses, US Patent, No: US3833347.

[6] http://www.toshiba-machine.co.jp/english/product/high/contents/molding.html

[7] Gy, R., Duffre`ne, L., Labrot, M., 1994, New insights into the viscoelasticity of glass, *Journal of Non-Crystalline Solids*, Vol. 175, pp. 103-117.

[8] Duffre`ne, L., Gy, R., 1997, Viscoelastic constants of a soda-lime-silica glass, *Journal of Non-Crystalline Solids*, Vol. 211, pp. 30-38.

[9] Duffre`ne, L., Gy, R., Burlet, H., Piques, R., 1997, Viscoelastic behavior of a soda-lime-silica glass: inadequacy of the KWW function, *Journal of Non-Crystalline Solids*, Vol. 215, pp. 208-217.

[10] Hyre, M., 2002, Numerical Modeling of glass forming and conditioning, *Journal of the American Ceramic Society*, Vol. 85, pp.1047-1056.

[11] Zhou, T., Yan, J., Masuda, J., Kuriyagawa, T., 2009, Investigation on the viscoelasticicity of optical galss in ultraprecision lens molding process, *Journal of Materials Processing Technology*, Vol. 209, pp. 4484-4489.

[12] Jain, A., Firestone, G. C., Yi, A. Y., 2005, Viscosity Measurement by Cylindrical Compression for Numerical Modeling of Precision Lens Molding

Process, *Journal of the American Ceramic Society*, Vol. 88, pp. 2409-2414.

[13] Jain, A., Yi, A. Y., 2005, Numerical Modeling of Viscoelastic Stress Relaxation During Glass Lens Forming Process, *Journal of the American Ceramic Society*, Vol. 88, pp. 530-535.

[14] Jain, A., Yi, A. Y., 2006, Finite element modeling of structural relaxation during annealing of a precision-molded glass lens, *Journal of Manufacturing Science and Engineering*, Vol. 128, pp. 683-690.

[15] Jain, A., Yi, A. Y., Xie, X., Sooryakumar, R., 2006, Finite element modeling of stress relaxation in glass lens moulding using measured temperature-dependent elastic modulus and viscosity data of glass, *Modeling and Simulation in Materials Science and Engineering*, Vol. 14, pp. 465–477.

[16] Yi, A. Y., Jain, A., 2005, Compression Molding of Aspherical Glass Lenses–A Combined Experimental and Numerical Analysis, *Journal of the American Ceramic Society*, Vol. 88, pp. 579-586.

[17] Chen, Y., Yi, A. Y., Su, L., Klocke, F., Pongs, G., 2008, Numerical simulation and experimental study of residual stresses in compression molding of precision glass optical components. *Journal of Manufacturing Science and Engineering*, Vol. 130, 051012 (9 pages), DOI:10.1115/1.2950062.

[18] Shott Co.,
2006, http://www.schott.com/optics_devices/german/download/tie-40_optical_glass_for_precision_molding.pdf

[19] Shelby, J. E., 2005, *Introduction to Glass Science and Technology*, second ed. The Royal Society of Chemistry, Cambridge, UK.

[20] Ohara Co., 2003, *Technical Information*.

[21] Scherer, G. W., 1986, *Relaxation in Glass and Composites*. Wiley, New York.

[22] Uhlmann, D. R., Kreidl, N. J., 1986, *Glass: Science and Technology, Volume 3, Viscosity and Relaxation*. Academic Press Inc., New York.

[23] Marc, 2008, *Marc Volume A: Theory and User Information*, MSC Software.

[24] Yan, J., Zhoua, T., Masudab, J., Kuriyagawa, T., 2008, Modeling high-temperature glass molding process by coupling heat transfer and viscous deformation analysis. *Precision Engineering*, Vol. 33, pp.150-159.

[25] Tool, A. Q., 1946, Relation between inelastic deformability and thermal expansion of glass in its annealing range, *Journal of the American Ceramic Society*, Vol. 29, pp. 240-253.

[26] Soules, T. F., Busbey, R. F., Rekhsom, S. M., Markovsky, A., 1987, Finite-element calculation of stresses in glass parts undergoing viscous relaxation, *Journal of the American Ceramic Society*, Vol. 70, pp. 90-95.

[27] Narayanaswamy, O. S., 1971, A Model of Structural Relaxation in Glass, *Journal of the American Ceramic Society*, Vol. 54, pp. 491-498.

[28] Scholze, H., 1990, *Glass - Nature, Structure and Properties*. Springer-Verlag, New York.

[29] Webb, S., Knoche, R., 1996, The glass-transition, structural relaxation and shear viscosity of silicate melts, *Chemical Geology*, Vol. 128, pp. 165-183.

[30] Sipp, A., Richet, P., 2002, Equivalence of volume, enthalpy and viscosity relaxation kinetics in glass-forming silicate liquids, *Journal of Non-Crystalline Solids*, Vol. 298, pp. 201-212.

[31] Moyhihan, C.T., Easteal, A. J., DeBolt, M. A., Wilder, J., Tucker, J., 1974, Dependence of the glass transition temperature on heating and cooling rate, *The Journal of Physical Chemistry*, Vol. 78, pp 2673-2677.

[32] Moyhihan, C.T., Easteal, A. J., DeBolt, M. A., Tucker, J., 1976, Dependence of the fictive temperature of glass on cooling rate, *Journal of the American Ceramic Society*, Vol. 59, pp. 12-16.

[33] DeBolt, M. A., Easteal, A. J., Macedo, P. B., Moyhihan, C.T., 1976, Analysis of structural relaxation in glass using rate heating data, *Journal of the American Ceramic Society*, Vol. 59, pp. 17-21.

[34] Hodge, I. M., Berens, A. R., 1982, Effect of annealing and prior history on enthalpy relaxation in glassy polymers. 2. Mathematical modeling, *Macromolecules*, 15, pp. 762-770.

[35] Ohara Co., 2004. http://www.oharacorp.com/pdf/elbal42.pdf

[36] Fujidie Co.,
2003, http://www.fujidie.co.jp/j/seihin/taimamou/material/pdf/lineup.pdf

[37] ISO 10110-2, 1996, Optics and optical instruments - Preparation of drawings for optical elements and systems - Part 2: Material imperfections - Stress birefringence, 1st ed., International Organization for Standardization.

[38] Wu, T. C., 2007, *Die Shape Optimization on Molding Process of Optical Glass Lens*, M.S. Thesis, Mechanical Engineering, National Chiao Tung University.

[39] Badeshia, H. K. D. H., 2002, *Differential scanning calorimetry*, Materials Science & Metallurgy, University of Cambrigde.
http://www.msm.cam.ac.uk/phasetrans/2002/Thermal2.pdf

APPENDIX A DIFFERENTIAL SCANNING CALORIMETRY (DSC) MEASUREMENT [39]

Differential scanning calorimetry (DSC) is a technique for measuring the energy necessary to establish a nearly zero temperature difference between a substance and an inert reference material, as the two specimens are subjected to identical temperature regimes in an environment heated or cooled at a controlled rate.

Figure A.1 and Figure A.2 show two types of DSC systems in common use. In heat-flux DSC, the sample and reference are connected by a low-resistance heat-flow path (a metal disc). The assembly is enclosed in a single furnace. Enthalpy or heat capacity changes in the sample cause a difference in its temperature relative to the reference. The temperature difference is recorded and related to enthalpy change in the sample using calibration experiments.

In the power-compensation DSC, the sample and the reference material are placed in independent furnaces. When the temperature rises or falls in the sample material, power (energy) is applied to or removed from the calorimeter to compensate for the sample energy. As a result, the system is maintained at a “thermal null” state at all times. The amount of power required to maintain system equilibrium is directly proportional to the energy changes occurring in the sample. A power-compensation DSC directly measures energy flow in and out the sample without complex calculation on the heat-flux.

Diamond DSC (PerkinElmer Inc.) used in this work is a power-compensation DSC. Its scanning temperature ranges from -170 to 730°C, with accuracy of ±0.1°C and precision of ±0.01°C. Scanning rates range from 0.01 to 500°C /min.

In this DSC measurement, heat flow is the measured value and specific heat

capacity is calculated by the following equation:

$$C_p = \frac{E \times H \times 60}{Hr \times M} \tag{A.1}$$

where C_p is the specific heat capacity (J/g/°C), E is the calibration constant (dimensionless), H is the heat flow (mw), 60 is the conversion constant (min to sec), Hr is the heating rate (°C/min) and M is the sample mass (mg).

The measuring procedures are as follows:

Firstly, an empty pan (usually using copper as the sample pan) was run to determine the background heat flow.

Second, heat the sapphire disc, which C_p is the standard value, at the temperature of interest to determine the calibration constant, E.

Lastly, perform third round of measurement on the sample. By using eq. (A.1) and the determined E, C_p of the sample is calculated.

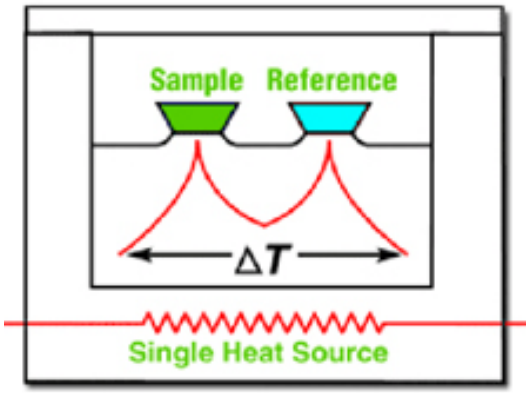

Figure A.1 Heat-flux DSC

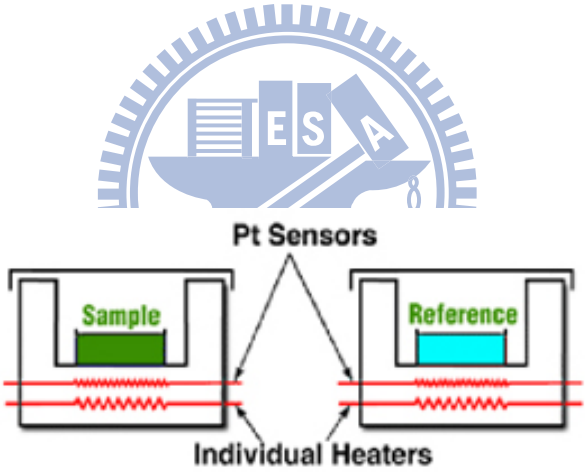

Figure A.2 Power-compensation DSC.